Surface Modified Fly Ash for Value Added Products (SuMo Fly Ash)

DOE Award Number: DE-FE0032039

Recipient: The Board of Trustees of the University of Illinois at Urbana-Champaign

Final Technical Report

Grant Period: September 1, 2021 to January 31, 2024

Principal Investigator
Chinmoy Baroi, PhD

Phone: 217-244-1709
Fax: 217-333-8944
Email: cbaroi@illinois.edu

University of Illinois
Unique Entity Identifier (UEI) Y8CWNJRCNN91

ATTN: Robin Beach
Sponsored Programs Administration
1901 South First St., Suite A
Champaign, IL 61820

Submitted to:

U. S. Department of Energy
National Energy Technology Laboratory

Project Manager: Adam Payne
Email: Adam.Payne@netl.doe.gov

Disclaimer

Contributing Authors

Sanandam Bordoloi; Linduo Zhao; Eric Devney; Peter Polyak, Katrina Cornish; Judit E. Puskas; Jeanne Norton; B K Sharma; Chinmoy Baroi

TABLE OF CONTENTS

LIST OF FIGURES

are indicated by solid red circle and black star symbols, respectively, except the data at their own pH are shown by open symbols.

LIST OF TABLES

EXECUTIVE SUMMARY

According to the U.S. Environmental Protection Agency, coal ash is a major contributor to U.S. industrial waste. Any use of fly ash, a primary component of coal combustion residuals (CCR) would have a significant impact on waste disposal if two conditions can be met: 1) fly ash residuals are cost-competitive with current materials; and, 2) contaminants in the coal ash can be encapsulated to eliminate problems related to leaching.

The American Coal Ash Association (ACAA) reported that in 2022, 28.2 million tons (Mt) of fly ash were produced and 16.8 Mt of fly ash were utilized. Also, there are regional imbalances in the supply and demand, leading to either a local oversupply or a deficit of fly ash. The ACAA also estimates that nationally, the gap between the demand and supply of concrete-grade fly ash is about 25%.

Existing uses for fly ash shown as Market Ready/Mature Technologies suffer from low value. In these applications, transportation and beneficiation costs of off-spec materials are key barriers to effectively utilizing existing supply. However, emerging applications such as the market for polymer fillers, extenders, and toughening agents, estimated to be about $10 billion, command higher prices. The benefits of developing higher-value uses for fly ash are to (a) expand the economic viability of transportation to greater distances to overcome regional supply-demand imbalances, (b) incentivize technologies to size, beneficiate, and store fly ash, and (c) create non-seasonal product demand. This project overcomes the barriers of previous research on the beneficial use of coal ash, by developing a new generation of biobased polymer-coated fly ash to eliminate user exposure to toxic elements. The project aims to characterize the polymer-modified fly ash to understand fundamental properties relevant to their performance as fillers in polymers.

The objective of this project is to develop a technology to encapsulate coal fly ash particles in sulfurized vegetable oil, enhancing physical and mechanical properties of the fly ash as a filler material when applied in commercial products. This project significantly advances the knowledge base and technology for synthesizing coated fly ash particles for application in different polymer matrices to increase cross-linking, compatibility, air-entrainment and to decrease the leaching potential of metals of concern. Specifically, the project focuses on (a) collection, and characterization of fly ash material from coal power plants; (b) development of Sulfurized Vegetable Oil (SVO) modified (SuMo) fly ash and their detailed characterization; (c) evaluation of the mechanical properties of the SuMo fly ash incorporated plastic and rubber composites for

potential replacement of $CaCO_3$ or carbon black as filler materials with SuMo fly ash in plastic and rubber composites; (d) leaching potential of SuMo fly ash and SuMo fly ash-incorporated plastic and rubber composites to determine the rate of release of trace metals.

The major findings of this project are: i) Sulfurized Vegetable Oil coated fly ash (SuMo fly ash) was successfully prepared with a particle size of ≤ 45 micron which exhibited hydrophobicity of contact angle > 90º; ii) the coating reduces leaching of metals (e.g., B, Cr) from fly ash when exposed to water; iii) incorporation of SuMo fly ash increases thermal stability and yield strength of plastics; iv) SuMo coating helps disperse fly ash particles into cured rubbers, natural rubber; (v) SuMo fly ash-incorporated plastic/cured rubbers compounds protects against leaching of toxic elements.

1. INTRODUCTION

The American Coal Ash Association (ACAA) reported that in 2022, 28.2 million tons (Mt) of fly ash were produced and 16.8 Mt of fly ash were utilized. Also, there are regional imbalances in the supply and demand, leading to either a local oversupply or a deficit of fly ash. The ACAA estimates that the gap between the demand and supply of concrete-grade fly ash is about 25% nationally.

Existing uses for fly ash shown as Market Ready/Mature Technologies in ***Figure 1***, are low value. In these applications, transportation and beneficiation costs of off-spec materials are key barriers to effectively utilizing existing supply (*EPRI, 2016*). However, emerging applications, such as the market for polymer fillers, extenders, and toughening agents, estimated to be about $10 billion, command higher prices.

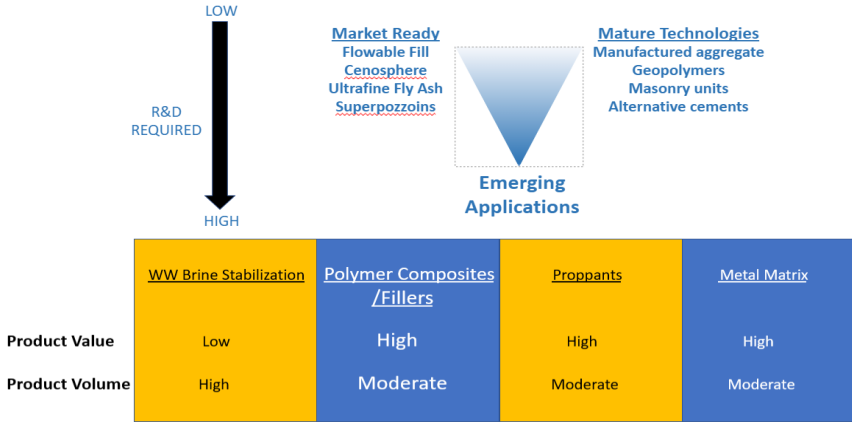

Figure 1. *EPRI (2016) analysis of Market Ready and Mature Technologies for fly ash utilization*

The benefits of developing higher value use for fly ash are to (a) expand the economic viability of transportation to greater distances to overcome regional supply-demand imbalances, (b) incentivize technologies to size, beneficiate, and store fly ash, and (c) create non-seasonal product demand.

Rationale: We embark on the proposed strategy based on the following identified advantages and disadvantages of as-is fly ash relative to other inorganic fillers in the current market (***Table 1***).

Table 1. *Advantages and disadvantages of the proposed modified fly ash as filler compared to inorganic fillers.*

Advantages
• Low cost relative to inorganic fillers • Aspect ratio close to spherical: not many natural materials have this characteristic; sphericity is advantageous in processing leading to a 30-70% less compounding time and tunable rheology • Density of fly ash is lower than calcium carbonate allowing for higher volumetric loading

Disadvantages	***Route to Mitigation in This Proposal***
Color: grey to black	*Choose applications where color is not an issue, e.g., rubber tires, black plastics.*
Multimodal size distribution	*Use sized fractions.*
Presence of elements such as As, Se, Cd, Hg	*Size, separate, encapsulate, and then use as filler; smaller size fractions tend to be enriched in As, Se, etc.*
Presence of OH groups; dispersion in nonpolar polymer matrices requires coupling agents such as silanols; smaller particles tend to agglomerate and lower impact strength	*Fly ash surface modification to increase hydrophobicity and allow better adhesion*
Tendency to pick up moisture; 2-20% moisture content; forms voids in hot molded products	*Hydrophobic modification to lower moisture pickup*

Environmental Benefits: Beneficial use of modified fly ash as fillers in plastic, elastomers, and thermosets can produce positive environmental and economic benefits by reducing the use of virgin resources, lowering greenhouse gas emissions, and reducing the cost of coal ash disposal. Also, the reduced leaching potential of the surface-modified (SuMo) fly ash will help to transform a low-value landfill waste to an inert material with application in high-value products. The diversion of fly ash from landfills, ash ponds, and impoundments will also reduce the risk of groundwater contamination.

Economic Benefits: Ground Calcium Carbonate (GCC) is the largest inorganic filler consumed in the market with about 10 million tons used by the plastics and paint sector. The market price of GCC is about $200/ton for untreated 3-7µm grades and about $300/ton for 1-3µm surface-treated grades. We expect the modified fly ash products to compete with $CaCO_3$ in applications that are not color sensitive and can benefit from reduced density, higher hardness, and increased interaction with nonpolar matrices. The price point of the modified fly ash product is expected to be competitive with GCC in substituted products.

The modified fly ash products are also expected to substitute partially for carbon black in rubber which is much more expensive than GCC. This market is large and growing.

2. COLLECTION, SIZING, AND CHARACTERIZATION OF FLY ASH MATERIAL

2.1. Collection and Sizing

Unclassified Class C and Class F fly ash were procured from Boral Resources. Class F fly ash was also collected from power plants burning Illinois coal to check for variations in elemental properties.

Fly ash was dried at 101°C for 16 hours to remove any moisture using the ASTM method D2974.

The dried fly ash was sieved through a series of meshes with a screen size of 75µm, 45µm, 10µm, and 2µm. The results of the fraction in mass percentages are presented in ***Figure 2***. There were no fractions less than 2µm and a tiny fraction (0.1-0.3%) less than 10µm. In all three Class F samples, the 45-75µm size fraction accounted for greater than 40% of the total fly ash mass. The 10-45µm size fraction accounted for 30-35% of the fly ash samples and the fraction greater than 75µm accounted for 18-23% of the fly ash samples. Class F fly ash of <3µm was also obtained from Boral Resources. The mass fraction of Class C fly ash is shown in ***Figure 3***.

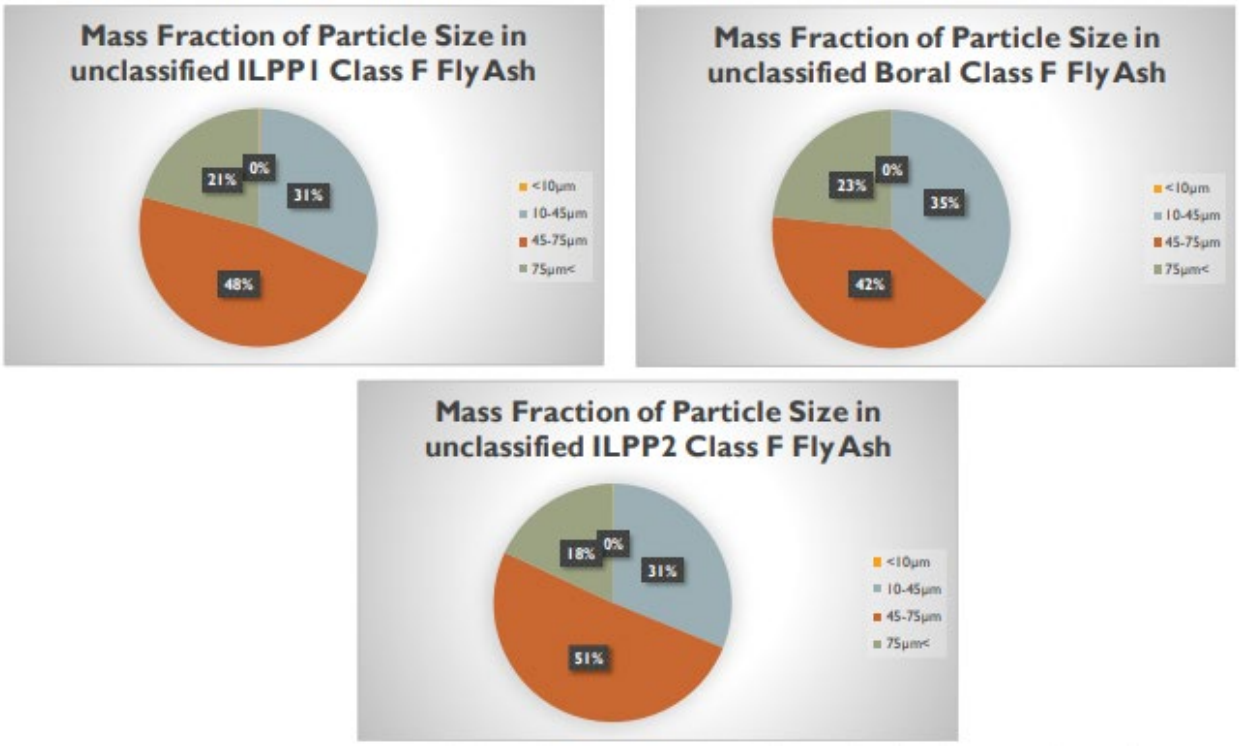

Figure 2. *Mass percentage of size fractions in unclassified Class F fly ash*

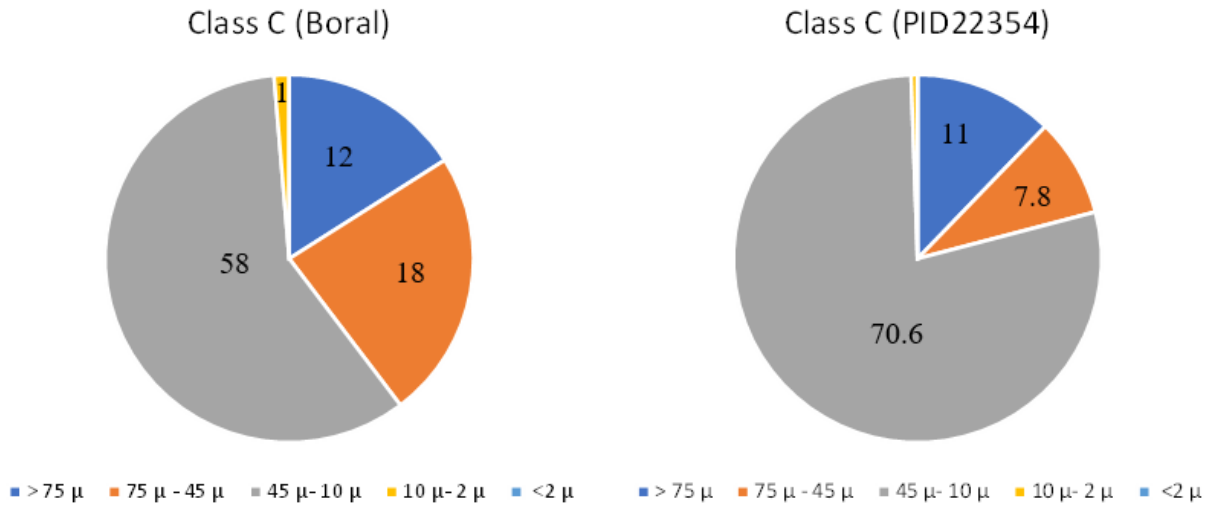

***Figure 3**. Mass percentage of size fractions in unclassified Class C fly ash*

2.2. Physical properties of fly ash

The physical properties of the size segregated fly ash fractions are listed in ***Table 2***.

***Table 2**. Physical properties of the size-segregated fly ash fractions*

Sample	Size fraction	Density (g/cc)	Porosity (%)	Specific gravity (G_s)	Void ratio (e)	Saturated liquid content, W (%)	Hygroscopic moisture (%)
Class F (Micron^3 Boral)	3 µm	0.86	66.7	2.59	0.40	15.45	NA
Class F (ILPP1)	>75 µm	0.79	65.30	2.28	0.40	17.33	0.60
	45-75 µm	1.10	54.30	2.45	0.35	14.36	0.30
	10-45 µm	1.10	58.70	2.56	0.37	14.45	0.20
Class F (ILPP2)	>75 µm	1.10	50.70	2.24	0.34	15.02	0.30
	45-75 µm	1.00	58.30	2.45	0.37	15.03	0.40
	10-45 µm	0.84	66.80	2.54	0.40	15.77	0.40
Class F (Boral)	>75 µm	1.30	52.40	2.7	0.34	12.73	NA
	45-75 µm	1.20	55.80	2.66	0.36	13.46	NA
	10-45 µm	1.00	61.00	2.69	0.38	14.08	NA
Class C (PP1)	>75 µm	0.99	56.90	2.30	0.36	15.90	NA
	45-75 µm	1.08	59.10	2.64	0.37	14.07	NA

	10-45 µm	1.18	51.00	2.41	0.34	14.01	NA
Class C (Boral)	>75 µm	1.17	53.70	2.53	0.35	13.81	NA
	45-75 µm	1.09	58.80	2.65	0.37	13.97	NA
	10-45 µm	1.14	56.60	2.63	0.36	13.74	NA

2.3. Fly Ash Morphology

Each of the size fractions was homogenized and made into a heap. The heap was divided into four quadrants. The sample from one quadrant was used for morphological and chemical analysis. Scanning Electron Microscope (SEM) analysis was conducted on the particles to study the particle morphology (***Figure 4***). Fly ash particles were well separated according to the expected size ranges, confirming the effectiveness of the size fractionation procedure in this study. The fly ash fraction of the finest size (<10µm) was noted to consist of primarily smooth spherical particles (***Figures 4-6***). Fly ash particles in size range of 10–45µm and higher included a significant number of irregularly shaped grains. These results are consistent with the previous studies (***Kutchko and Kim 2006***; ***Yüksel and Yürüm 2009***, ***Zhu et al. 2013***).

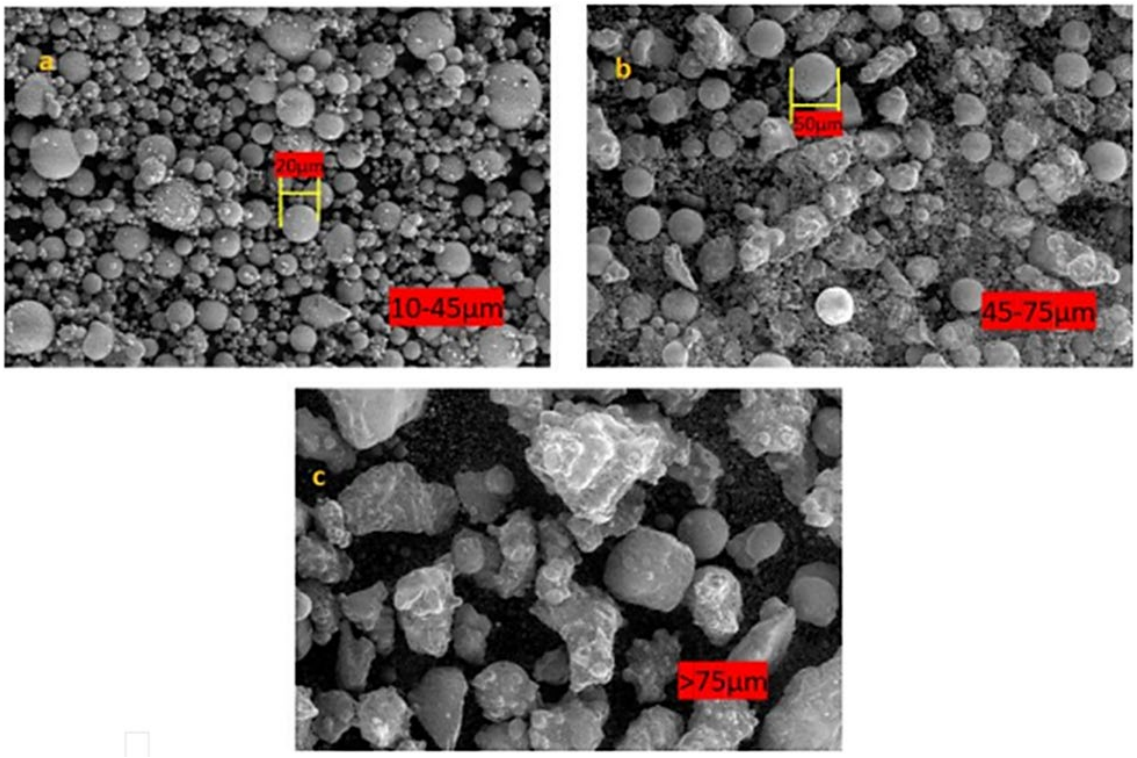

Figure 4. *SEM Images of size-segregated Boral unclassified Class C fly ash: a) fraction with particle size 10-45µm; b) fraction with particle size 45-75µm); c) fraction >75µm*

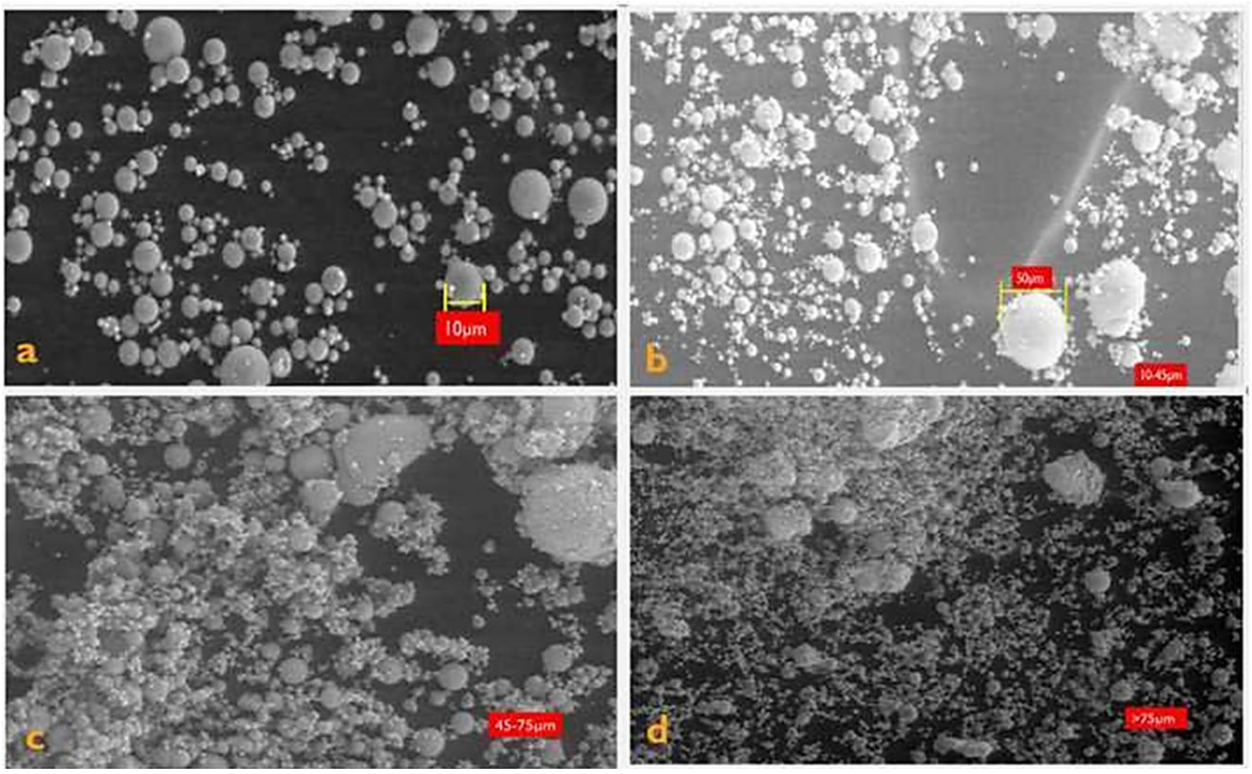

Figure 5. *SEM Images of size segregated Boral unclassified Class F fly ash:* ***a)*** *fraction with particle size <10µm;* ***b)*** *fraction with particle size 10-45µm;* ***c)*** *fraction with particle size 45-75µm);* ***d)*** *fraction >75µm*

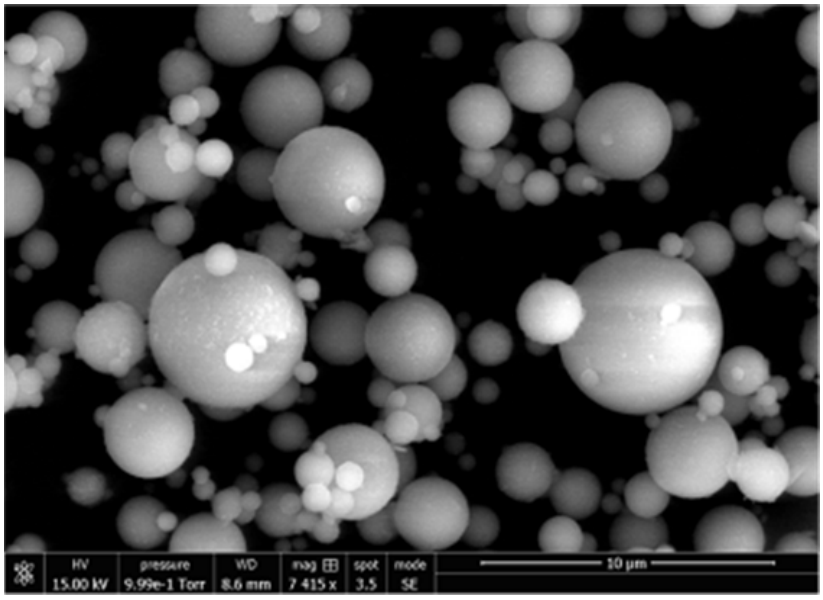

Figure 6*. SEM Image of Boral Micron*[3]

The fly ash sample from PP1 had a loss on ignition of 20% on particles larger than 75µm (***Table 3***). This indicates the presence of unburnt carbonaceous material in PP1.

Table 3. *Loss on ignition on the size segregated fly ash fractions*

Sample	Size fraction	Loss on ignition (%)	
		550 ℃	**750** ℃
Class F (Micron^3 Boral)	3 µm	0.2	0.2
Class F (ILPP1)	75 µm	**11.3**	**12.4**
	45-75 µm	2.7	2.7
	10-45 µm	1.8	1.8
Class F (ILPP2)	75 µm	0	0.5
	45-75 µm	0	0.7
	10-45 µm	0	0.9
Class F (Boral)	75 µm	0.4	0.4
	45-75 µm	0.5	0.5
	10-45 µm	0.6	0.6
Class C (PP1)	75 µm	**21.7**	**26.3**
	45-75 µm	**9.2**	**9.9**
	10-45 µm	1.4	1.6
Class C (Boral)	75 µm	1.3	1.4
	45-75 µm	0.3	0.3
	10-45 µm	0.3	0.3

2.4. Elemental Composition

Major oxides were analyzed by X-Ray Fluorescence (XRF), and the results are tabulated in ***Table 4***. Fly ash consists primarily of oxides of silicon, aluminum, iron, and calcium. Other elements such as potassium, sodium, and sulfur are also present to a lesser degree. When used as a mineral admixture in concrete, fly ash is classified as either Class C or Class F ash based on its chemical composition. Class C ashes are generally derived from sub-bituminous coals and consist primarily of calcium aluminosulfate glass and quartz, tricalcium aluminate, and free lime (CaO). Class C fly ash is also referred to as high calcium fly ash because it typically contains more than 18% CaO. The results confirm that the Boral sample and the PP1 sample conform to the nomenclature.

***Table 4**. XRF analysis on the size segregated fly ash fractions*

Sample	Size fraction	Elemental oxides (%)						
		(i)	(ii)	(iii)	(iv)	(v)	(vi)	(i)+(ii)+(iii)
		SiO_2	Al_2O_3	Fe_2O_3	CaO	K_2O	SO_3	
Class F Micron[3] Boral	3 µm	55.29	17.57	5.58	9.91	4.05	1.46	**78.44**
Class F (ILPP1)	75 µm	49.01	15.75	13.15	13.11	2.28	***5.35***	**77.91**
	45-75 µm	55.87	16.58	14.16	7.16	2.08	3.13	**86.61**
	10-45 µm	56.92	16.4	13.62	6.42	2.17	3.37	**86.94**
Class F (ILPP2)	75 µm	54.8	19.33	9.47	8.96	3.82	1.86	**83.6**
	45-75 µm	54.57	19.36	9.21	9.16	3.91	1.91	**83.14**
	10-45 µm	54.34	18.89	9.32	9.55	4.05	1.98	**82.55**
Class F (Boral)	75 µm	40.41	20.70	5.41	**27.4**	1.01	1.66	66.52
	45-75 µm	39.7	20.58	5.70	**27.86**	1.06	1.58	65.98
	10-45 µm	39.93	20.85	5.43	**27.66**	1.05	1.61	66.21
Class C (PP1)	75 µm	24.3	9.8	17.9	**18.9**	1.3	***22.1***	49
	45-75 µm	41.5	15.8	17.8	**14.0**	1.7	***6.0***	**75.1**
	10-45 µm	34.7	14.4	16.8	**24.1**	1.6	4.1	65.9
Class C (Boral)	75 µm	33.5	15.5	9.9	**29.5**	1.1	2.6	58.9
	45-75 µm	34.4	15.4	9.2	**28.6**	1.0	2.3	59
	10-45 µm	29.0	14.4	10.0	**30.0**	0.9	2.2	53.4

2.5. Minor/Trace Elements by Inductively Coupled Plasma Mass Spectroscopy (ICP-MS)

Trace metal analyses were conducted by digesting the size-segregated fly ash sample and subsequently analyzed by ICP-MS. Mercury was analyzed using cold vapor atomic absorption (CVAA). These results are summarized in ***Tables 5*** and ***6***. Highly leachable elements like Boron and Manganese were found in substantial concentrations. Mercury (Hg) was not detected in either of the Class C and F samples.

***Table 5**. Trace metal analysis on the size segregated Class C fly ash samples*

Elements	Units	Boral Unclassified Class C Fly Ash			PP1		
		>75µm	**45-75µm**	**10-45µm**	**>75µm**	**45-75µm**	**10-45µm**
As	mg/kg	13	17	16	17	24	38
Ba	mg/kg	4600	4370	5150	2020	2460	2050
Be	mg/kg	ND	ND	ND	ND	ND	ND
B	mg/kg	423	565	619	347	455	736
Cd	mg/kg	ND	1	1	ND	ND	1
Cr	mg/kg	52	69	69	46	56	84
Co	mg/kg	19	22	21	15	16	22
Cu	mg/kg	291	243	515	206	174	179
Pb	mg/kg	26	39	44	15	23	39
Mn	mg/kg	175	202	212	115	131	167
Mo	mg/kg	16	23	22	47	62	94
Ni	mg/kg	51	54	51	308	324	434
Se	mg/kg	4	4	4	3	4	4
Ag	mg/kg	ND	ND	ND	ND	ND	ND
Sn	mg/kg	BD	BD	BD	BD	BD	BD
V	mg/kg	179	228	225	1010	1160	1600
Zn	mg/kg	97	106	133	76	87	119
Hg	mg/kg	BD	BD	BD	BD	BD	BD
Al	mg/kg	64800	75800	81000	48600	49200	70800

***ND- Not Detected**
***BD- Below Detection Limit**

***Table 6**. Trace metal analysis on the size segregated Class F fly ash samples*

Elements	**Units**	**Micron 3 Boral Fly Ash**	**ILPP1 Fly Ash (µm)**			**ILPP2 Fly Ash (µm)**			**Boral Unclassified Class F Fly Ash (µm)**		
		3 µm	**>75**	**45-75**	**10-45**	**>75**	**45-75**	**10-45**	**>75**	**45-75**	**10-45**
As	mg/kg	**158**	12	14	17	15	22	24	18	21	22
Ba	mg/kg	1630	177	172	145	306	345	287	3420	3180	3390
Be	mg/kg	3	5	5	6	BD	BD	BD	3	3	3
B	mg/kg	1040	992	1190	1720	403	548	597	522	603	616
Cd	mg/kg	2	4	4	5	3	4	5	2	2	2
Cr	mg/kg	90	56	63	78	109	145	157	60	69	70
Co	mg/kg	11	7	6	6	4	5	5	25	28	29
Cu	mg/kg	58	32	51	95	41	46	67	151	212	244
Pb	mg/kg	**60**	10	10	16	7	11	13	34	43	45
Mn	mg/kg	**246**	567	415	292	121	108	91	146	151	155
Mo	mg/kg	20	28	31	38	28	39	44	10	12	13
Ni	mg/kg	29	30	30	32	26	31	31	51	56	57
Se	mg/kg	15	20	12	10	20	29	33	8	11	12
Ag	mg/kg	ND	ND	ND	ND	ND	ND	ND	ND	ND	ND
Sn	mg/kg	5	3	3	5	2	3	3	4	4	4
V	mg/kg	137	102	92	118	78	102	108	154	166	174
Zn	mg/kg	113	231	168	219	134	180	208	155	177	180
Hg	mg/kg	ND	0.84	ND	ND	ND	ND	ND	1	1.5	1.6

3. DEVELOPMENT OF A SURFACE COATING TECHNIQUE TO GENERATE MODIFIED FLY ASH (SUMO)

3.1. Synthesize Sulfurized Vegetable Oil Followed by Coating

For the dry coating method – 1g of canola oil was sulfurized with (0.2g) sulfur at 165°C for 20 minutes until all the sulfur was reacted with oil to form a dark brown thick viscous liquid. (See ***Figure 7***) The fly ash (1g) was then manually mixed with 0.1g of sulfurized vegetable oil (SVO) without any solvent. This material was then cured at 165°C for 45 minutes.

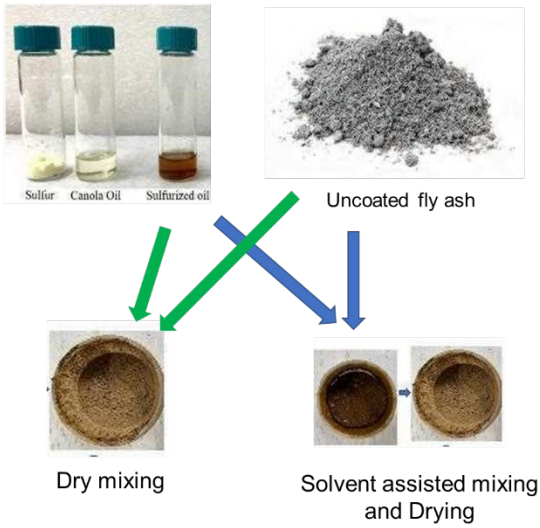

Figure 7*. SuMo fly ash generation by synthesizing sulfurized vegetable oil followed by coating*

For coating using solvent – 1g of canola oil was sulfurized with (0.2g) sulfur at 165°C for 20 minutes until all the sulfur was reacted with oil to form a dark brown thick viscous liquid. About 0.1g of sulfurized vegetable oil (SVO) was dissolved in toluene (5 mL). The fly ash (1g) was then slurried in this mixture and then vacuum evaporated until all the solvent was removed. This material was then cured at 165°C for 45 minutes. Both the conductivity and the pH were substantially reduced on coating with sulfurized vegetable oil (SVO) with and without solvent. The conductivity, however, slightly increased at the end of 24 hours (***Figure 8***, y-axis; log scale) and remained constant for the next 24 hours. The error bars on the graphs indicate standard deviation from triplet runs. All of the experiments were repeated three times at least for reproducibility. This indicates that the coating is more stable. However, the particles were larger. SEM imaging (***Figure 9***) revealed that the particles had agglomerated to form large particles of about 0.5-1mm in size.

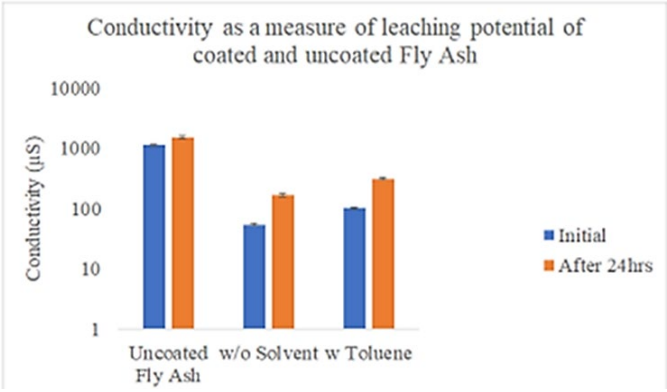

Figure 8*. Leaching of uncoated and coated SuMo fly ash samples*

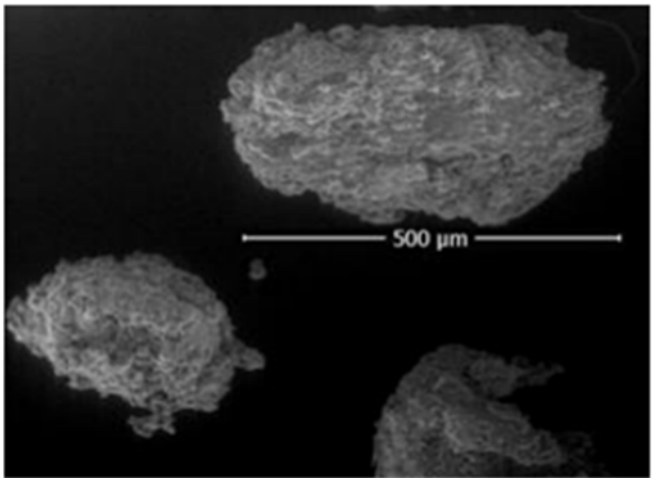

Figure 9. *SEM image of SVO-coated fly ash*

3.2. Sulfurization of Vegetable Oil-Coated (SVO) Fly Ash

For dry method fly ash was prewetted with canola oil without addition of any solvent and mixed well. (See ***Figure 10***) The prewetted fly ash was then mixed with clear molten sulfur at 165°C and then stirred until a dark brown color was obtained. This material was then cured at 165°C for 45 minutes. The difference between the solvent and nonsolvent was that oil was dissolved into the solvent (Toluene) and then fly ash was mixed with this oil/solvent mixture and dried until solvent was completely evaporated. This material was then cured at 165°C for 45 minutes. Again, a similar observation was made as to that of the previous method. The coating reduced the leaching by an order of magnitude (***Figure 11***). The error bars on the graphs indicate standard deviation from triple runs. All the experiments were repeated three times at least for reproducibility. Initial conductivity was 1,000µs for uncoated fly ash but was less than 100 after coating. At the end of 24 hours the conductivity was about 200µs using both methods. However,

Figure 10. *SuMo fly ash generation by sulfurization of vegetable oil (SVO) coated fly ash*

particle size was visually larger than the initial fly ash. The particles were agglomerated to form large particles of about 1mm in size (***Figure 12***).

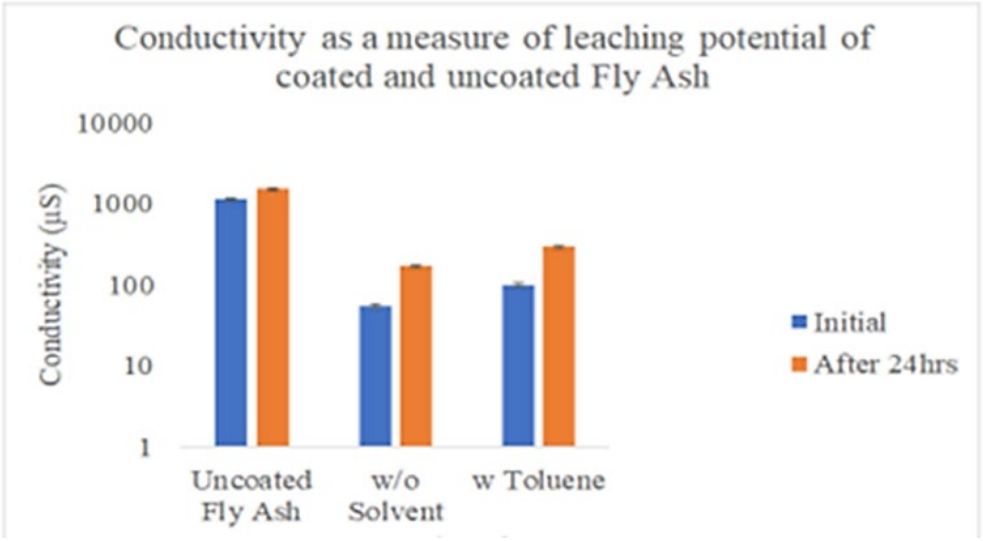

Figure 11. *Leaching of uncoated and coated SuMo fly ash samples*

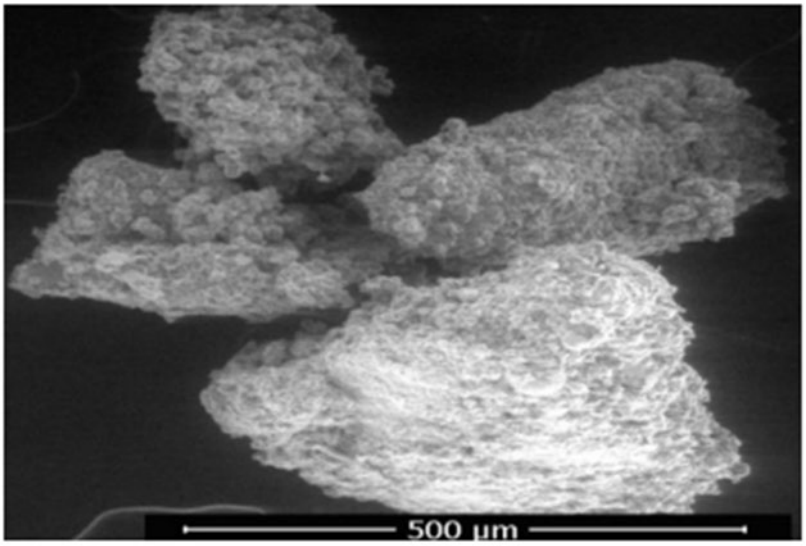

Figure 12*. SEM image of SVO coated fly ash*

3.3. Optimization of Conditions to Generate SuMo Fly Ash

The development of the SuMo fly ash involved three stages: (1) Development of crosslinked polymer from S and Oil by inverse vulcanization; (2) Coating of the crosslinked polymer on the FA; and (3) Analysis of developed SuMo fly ash conforming to an idealized filler. Thermal homolysis of S-S bonds leads to radical ring-opening polymerization **(*Worthington et al., 2017*)**. Subsequent trapping of the thiyl radical end groups of the sulfur polymers with a polyene resulted

in a cross-linked polysulfide polymer. The alkene functional groups in canola oil also provided the requisite points for cross-linking during inverse vulcanization (***Worthington et al., 2017***). Two parameters (i.e., S-to-Oil ratio, reaction condition (temperature) and curing conditions (temperature and time) were optimized to get an ideal polymer. In the first step, canola oil was reacted with elemental sulfur at 160°C for approximately 20-30 minutes until all the S dissolves and reacted to form a single-phase solution in the form of a flowable viscous polymer termed as sulfurized vegetable oil (SVO). The synthesis of SVO in the form of polysulfides by inverse vulcanization involved the melting of elemental sulfur and consequent heating of it above its floor temperature of 160ºC (***Dixon, 1985***). The S-Oil ratio was restricted to 15-100 ratio (by weight) for the current coating process as beyond this point the developed SuMo FA tended to be tacky and agglomerate. The S and oil reacted at 160ºC for approximately 15 minutes in an oil bath. The fly ash was initially washed with deionized water at L/S ratio of 5 two or three times to minimize the leaching potential before coating with SVO. The SVO upon curing tends to form rubbery hydrophobic polymer. The toughness of the cured polymer was assessed through a durometer (***Ghosh and Karak, 2018***) and the highest durometer reading at different curing conditions was chosen for curing the polymer on the fly ash. Based on initial trial tests, curing at 160ºC for 15 hours resulted in a polymer with highest durometer reading.

The SVO was coated on the fly ash with the intention that the produced SuMo (SO) fly ash would essentially be hydrophobic, have particles that would ideally retain the original spherical morphology of the fly ash as well as the small particle size (minimized agglomeration due to polymer). The coating involves a two-step simultaneous mixing-curing-crushing stages (***Figure 13***). The first mixing was labelled as wet mixing wherein the washed fly ash was mixed with 15% SO (by weight of fly ash) using a solvent (toluene). The mixture was shaken in an orbital shaker for 16 hours to ensure that SVO engulfs the fly ash. After this mixing process, the excess toluene was evaporated by putting in a flume head and the wet fly ash was kept at 160ºC for 15 hours in an oven such that the encapsulated fly ash cures atop the fly ash. After the curing process, the samples were crushed in an in-house ball mill (Glen Mills GY-RO Mill 3/4HP Mill) for 5 seconds to break any agglomeration. Thereafter, the second mixing named as dry mixing involved mixing 3 to 7% SO with the coated samples from wet mixing stage. This mixing was done in a planetary centrifugal bubble free mixer (Model: ARE-310; Thinky Corporation) wherein it was mixed 4

times at 2,000 RPM for 2 minutes in each cycle. The mixed samples were cured at 160ºC for 15 hours followed by same crushing approach used in the wet mixing stage.

Figure 13. *SuMo fly ash generation by a two-step process*

Later, various other oils and fatty acids were explored to find out the optimum curing condition and S/Oil ratio based on polymer toughness (durometer reading) for different oil types. Details of the optimization results are listed in ***Table 7***. There were no polymers formed for the Oleic acid and Base 44.

Table 7. *Optimum curing conditions for polymer*

Oil type	S/Oil ratio	Curing temp	Curing time (h)
Canola	15/100	150	18
Soybean	15/100	180	24
Castor	15/100	150	18
Linseed	15/100	180	24
Oleic acid	NA	NA	NA
Base 44	NA	NA	NA

The second stage of DOE was to find optimum coated fly ash for each oil based on economy (i.e., lowest SVO to fly ash ratio; 10%, 12.5% and 15%) provided they pass through three criteria (leaching reduction by 70%, hydrophobicity, and yield of particles lower than 45µm at 70% yield). See ***Table 8*** for the optimum SVO/fly ash ratio with lowest conductivity values.

Table 8. *Optimum sulfurized vegetable oil to fly ash ratio by weight for SuMo fly ash*

Oil type	Class F (Micron^3)	Class C (Boral <45 µm)
Canola	15%	15%
Soybean	15%	15%
Castor	12.5%	15%
Linseed	15%	15%

Also, Class F fly ash responds better to the coating than Class C in terms of leaching suppression.

3.4. Characterization of SuMo Fly Ash

The produced SuMo fly ash exhibited hydrophobicity with a contact angle of 125° regardless of the coating conditions. This contact angle was also observed for the cured polymer (***Figure 14***). FE-SEM micrographs of fly ash indicate that all particles were spherical with particle size lower than 3µm (***Figure 14***). The hydro-dynamic diameter observed from particle size analysis was 1.32µm, which is like those observed in the micrographs and reported in previous literature (***Ren and Sancaktar, 2019***). ***Figure 15*** depicts that the SuMo fly ash also showed predominantly spherical particles with lower than 5µm. It appears that the overall constituents of finest spheres (say lower than 1µm) in SuMo fly ash were found to be lower than that of the uncoated fly ash. This may be due to the coating engulfing multiple fine spheres of less than 1µm into relatively bigger sized spheres (average hydrodynamic diameter was 2.34µm). The results indicate the milling process did not destroy the spherical particles into irregular shaped particles as reported by ***Ren and Sancaktar (2019)*** for the same fly

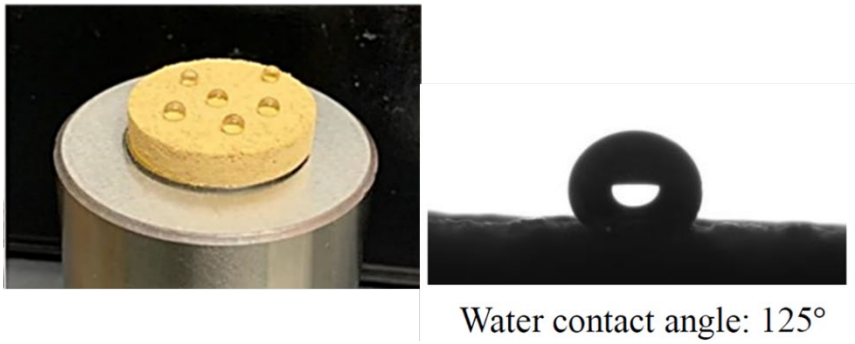

Figure 14. *SuMo fly ash hydrophobicity and contact angle measurement*

ash. From the micrographs, it was evident that the SVO coating on the fly ash did not alter the spherical shape of the individual FA particles but moderately reduced the relatively well graded particle size distribution of fly ash particles into particles having a uniform particle size distribution.

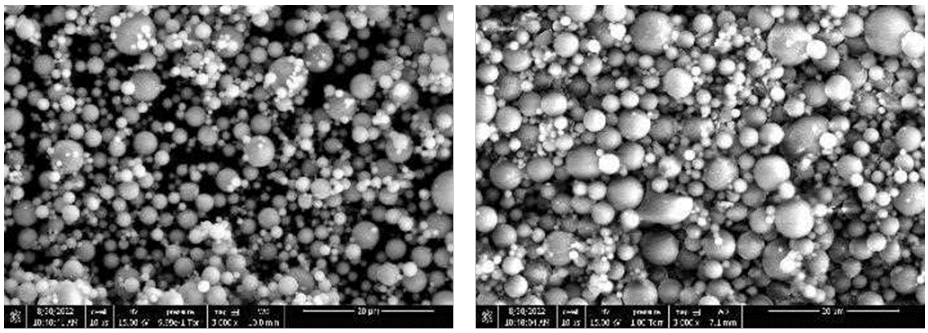

Figure 15. *SEM images of uncoated and SuMo fly ash*

Figure 16 presents the weight loss of SVO, uncoated FA and SuMo fly ash at different temperatures. The temperature range considered was below 500°C as, for composite molding, the temperature was generally within 160-250°C. As expected, the fly ash was thermally stable within that range of interest with no appreciable weight loss. At higher temperatures, up to 750°C, only 0.2% degradation happens and volatiles of around 2.4% were observed at around 900°C. The SuMo fly ash was stable thermally up to 300°C with no weight loss observed. However, beyond 350°C, there was an appreciable decrease in the material weight which is associated with the breakdown of the SVO. The SVO breaks down at 300°C and naturally the cured SVO will have higher thermal stability than the uncured SVO.

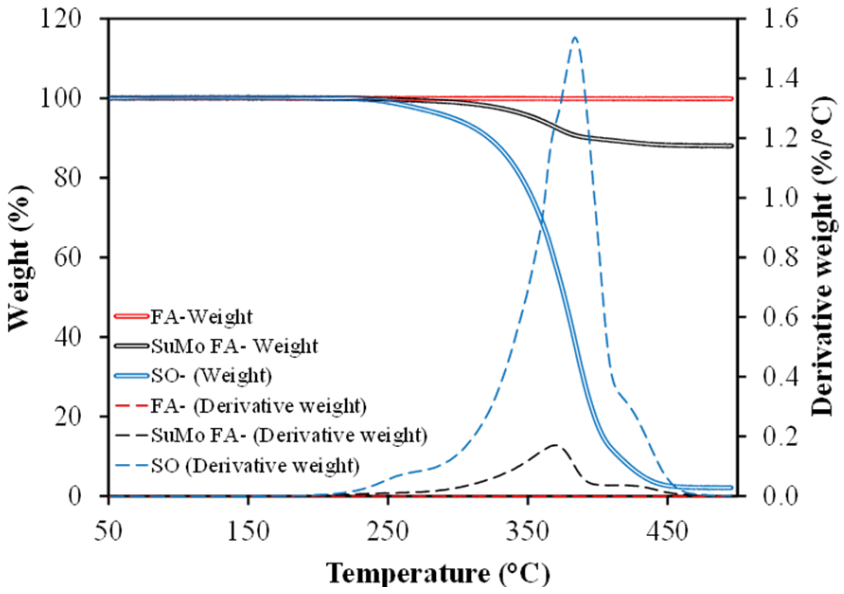

Figure 16. *TGA of uncoated and SuMo fly ash*

Figure 17 presents the FTIR spectra in terms of the surface functional groups in FA and SuMo fly ash. Some of the major consequences of the coating of the cross-linked polysulfide polymer on

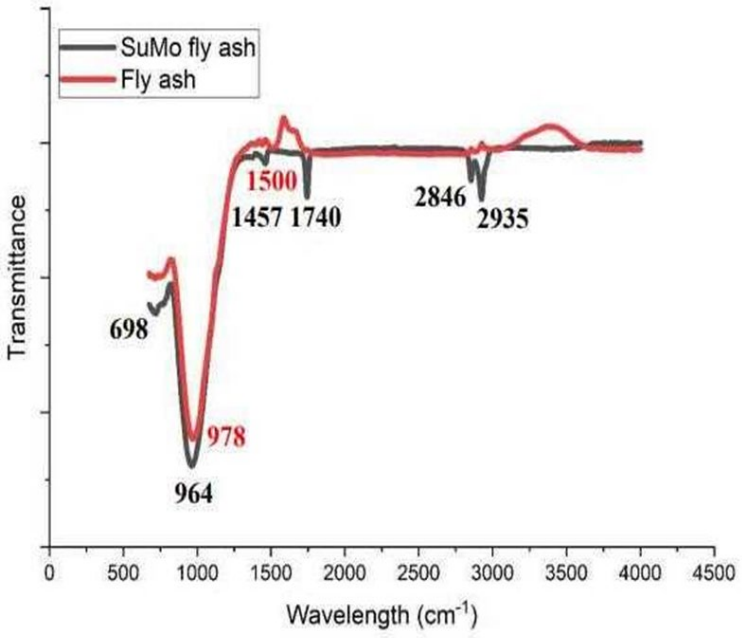

Figure 17. *FTIR spectra of uncoated and SuMo fly ash*

the fly ash resulted in distinct peaks appearing at 964cm^{-1} attributed to formation of C-S bond (***Nishal et al., 2013***). The distinct peak in 1740cm^{-1} observed in SuMo fly ash was attributed to the formation of non-conjugated ester unit due to the establishment of the polymer on the fly ash surface (***IkhtiarBakti and Gareso, 2018***). The distinct asymmetric bending peaks at 1457cm^{-1} clearly indicate the formation of C-H groups. The distinct bands between 2930-2900cm^{-1} also indicate the presence of C-H groups exhibiting asymmetrical stretching.

Figure 18 presents the AFM image of fly ash and SuMo fly ash presented at the same scale of reference. The fly ash showed an intricate surface without any irregularities conforming to the spherical shape of individual particles. On the other hand, the SuMo fly ash was relatively irregular due to the coating. However, both sample surfaces are in nano scale and thus the coating should ideally not translate into changes in mechanical properties when integrated into the polymer matrix. To investigate whether the coating was established on the fly ash particles, EDS spectra of fly ash and SuMo fly ash were obtained (***Figure 19***). The elemental composition clearly indicates a sharp increase in C and S in the SuMo fly ash, which suggests that the polysulfide polymer has likely encapsulated the fly ash particle.

The EC and pH of the leachate emanating from uncoated Micron^{3} fly ash after 24-hour tumbling condition in

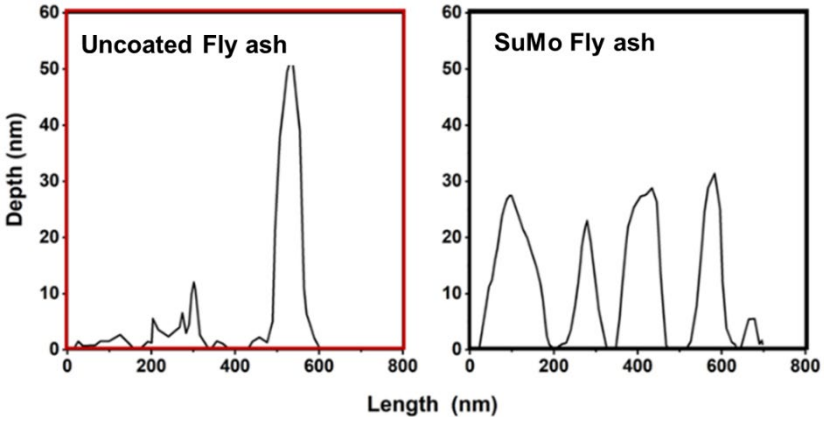

Figure 18. *Atomic force microscopy (AFM) micrographs of uncoated and SuMo fly ash*

deionized water were at 3,000 ±350 µS/m and 12.5 ±0.4, respectively. Fly ash consists of alkaline oxides present which can leach readily through diffusion and change the EC and pH of deionized water (***Khosla et al., 1979***; ***Roy and Berger, 2011***). The EC and pH of the SuMo fly ash under the same conditions of tumbling were at 550 ±150 µS/m and 8 ±0.5, respectively. Thus, the average range of per-centage reduction in EC for SuMo fly ash as compared to uncoated fly ash was at 75-87%, indicating a significant decrease of alkaline oxides. A decrease in pH by 4 units indicates that leachable calcium oxides did not diffuse into the water medium because of coatings. ***Figure 20*** presents the elemental concentration of selected elements (including some contaminants of potential concern (COPCs) using ICP-MS. It can be observed that all elements in the leachate of SuMo fly ash were lower than that of uncoated fly ash or were below the detection limit. The leachate of uncoated fly ash was higher than the EPA regulatory limit for these 12 elements. This drop to permissible limits after the fly ash was coated happened to all elements except for As. Major COPCs such as B, Cr, Pb, and Sr showed a decrease by more than one order. The observed decrease in EC, pH, and elemental leaching of COPCs for SuMo fly ash was expected to be further enhanced when the SuMo fly ash was integrated into the polymer matrix, which will further provide another layer against exposure to water.

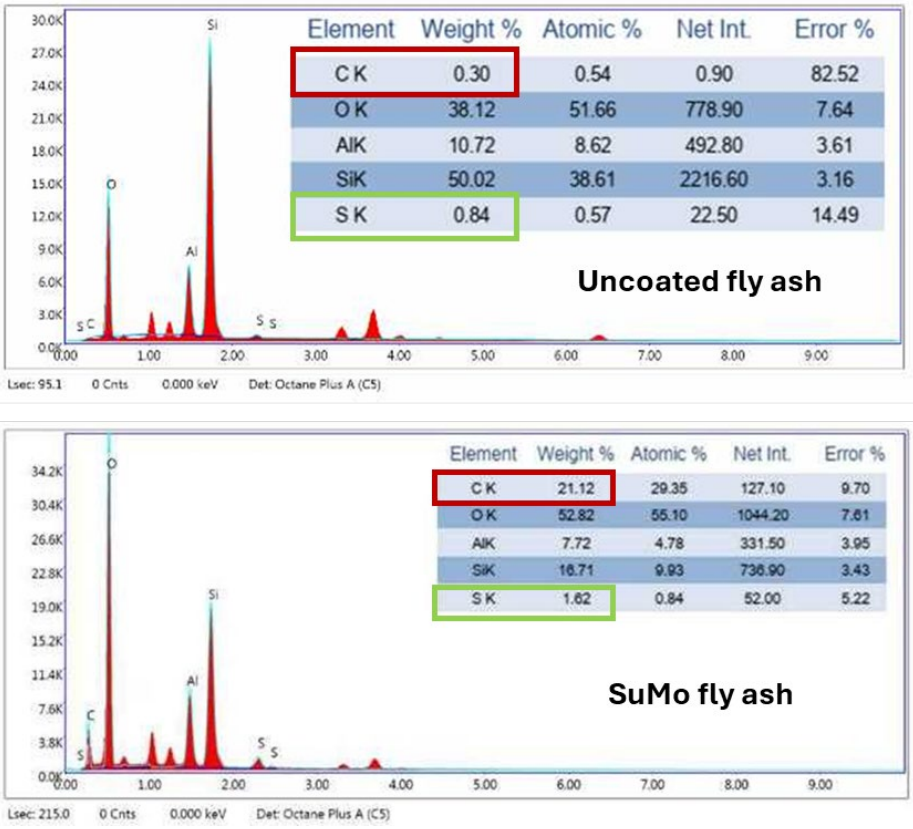

Figure 19. *EDS spectra of uncoated and SuMo fly ash*

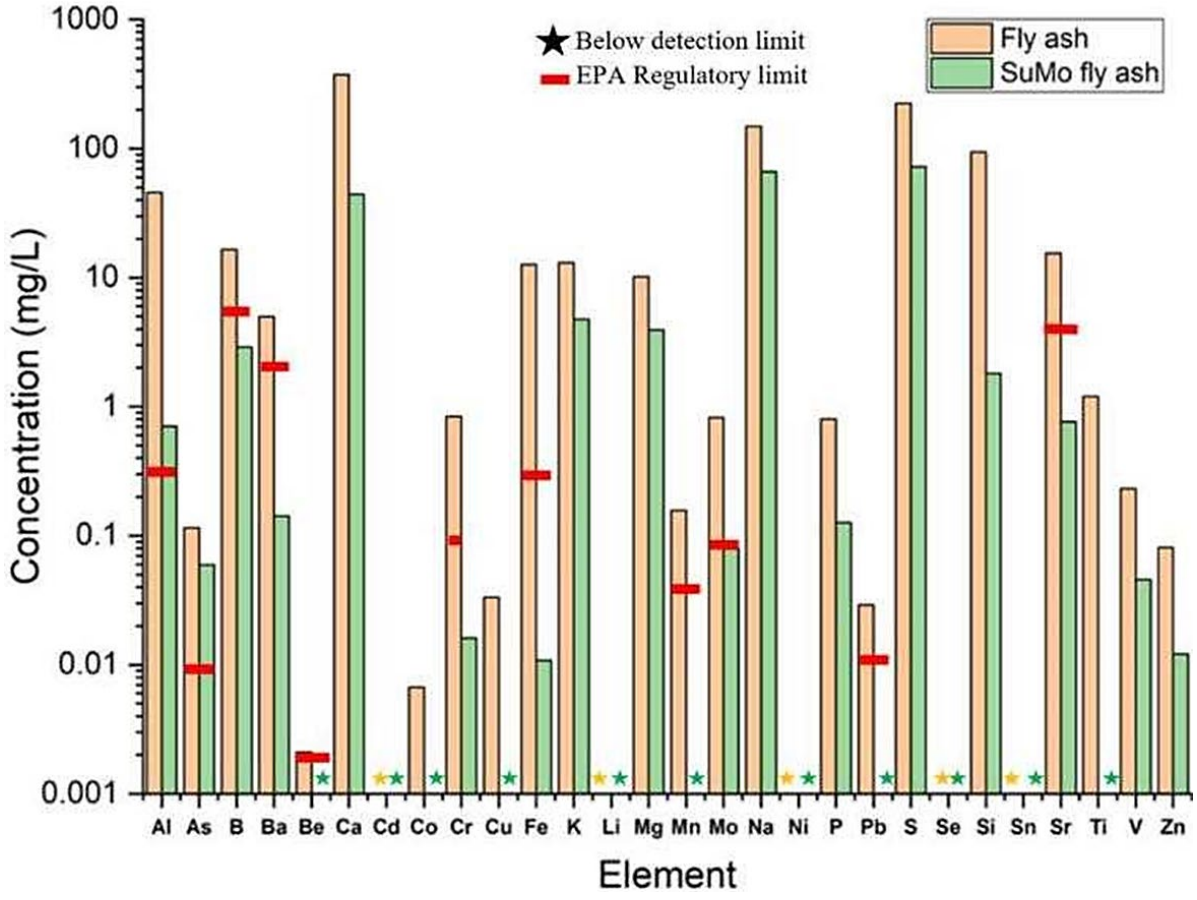

Figure 20. *Elemental concentration of leachate for uncoated fly ash and SuMo fly ash*

4. SUITABILITY OF SUMO FLY ASH AS FILLER MATERIAL IN PLASTICS/CURED RUBBERS

4.1 Replacement of $CaCO_3$ Filler in Plastics

Fly ash, SuMo fly ash and $CaCO_3$ were compounded within the polypropylene (PP) and polyethylene (PE) matrix first in the form of pellets and then injection molded into test bars. The filler percentage weight with respect to polymer compounded was kept at 20% for comparison. LabTech twin-screw extruder was used to make pellets. The test bars were prepared using an Arburg 320 S Allrounder injection mold machine at the temperature range of 205°C with cycle time, cooling time, holding time, and shot size of 75s, 40s, 15s and 6.9cm, respectively.

The $CaCO_3$ filled PP and PE thermoplastics retained their white color. On the other hand, the unmodified fly ash and SuMo fly ash filled thermoplastics had dark yellow (Class F) /grey (Class C) and brown color, respectively (***Figures 21-22***).

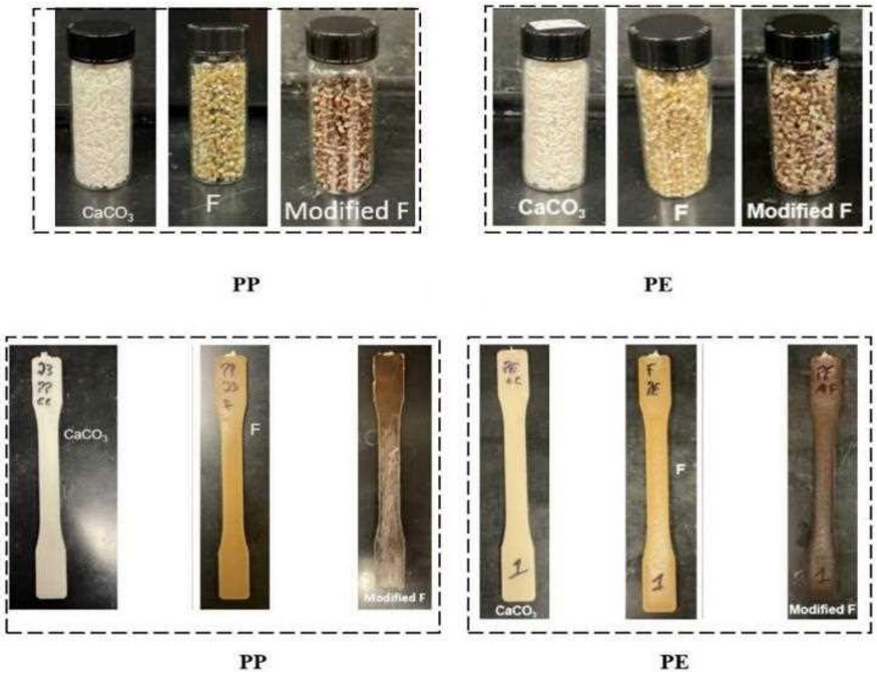

Figure 21*. Unmodified Class F, SuMo Class F and $CaCO_3$ incorporated PP and PE thermoplastics test bars*

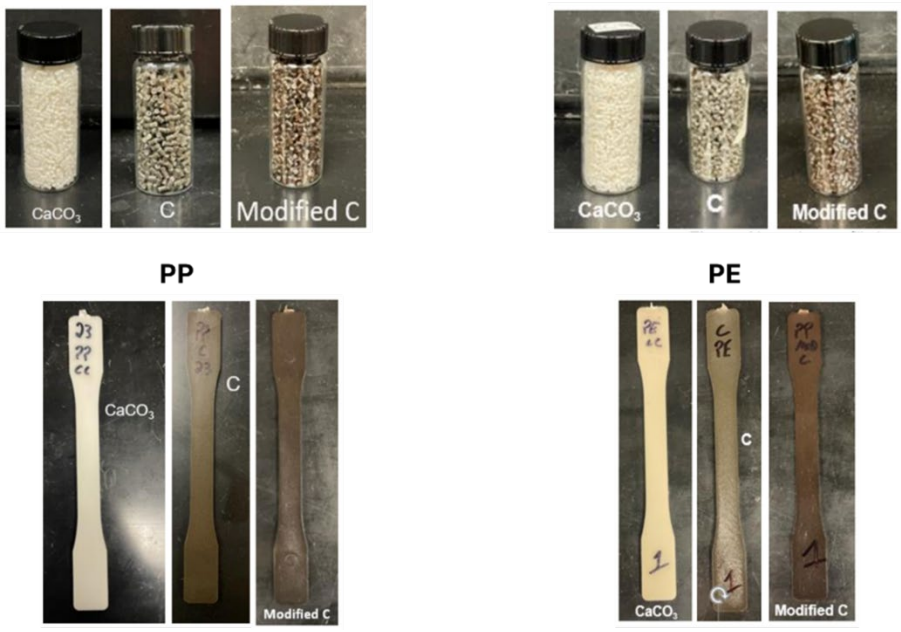

***Figure 22**. Unmodified Class C, SuMo Class C and $CaCO_3$ incorporated PP and PE thermoplastics test bars*

Figures 23–26 show that surface coating of fly ash (SuMo fly ash) helps well dispersion of fly ash into the PP and PE thermoplastics as compared to the unmodified fly ash.

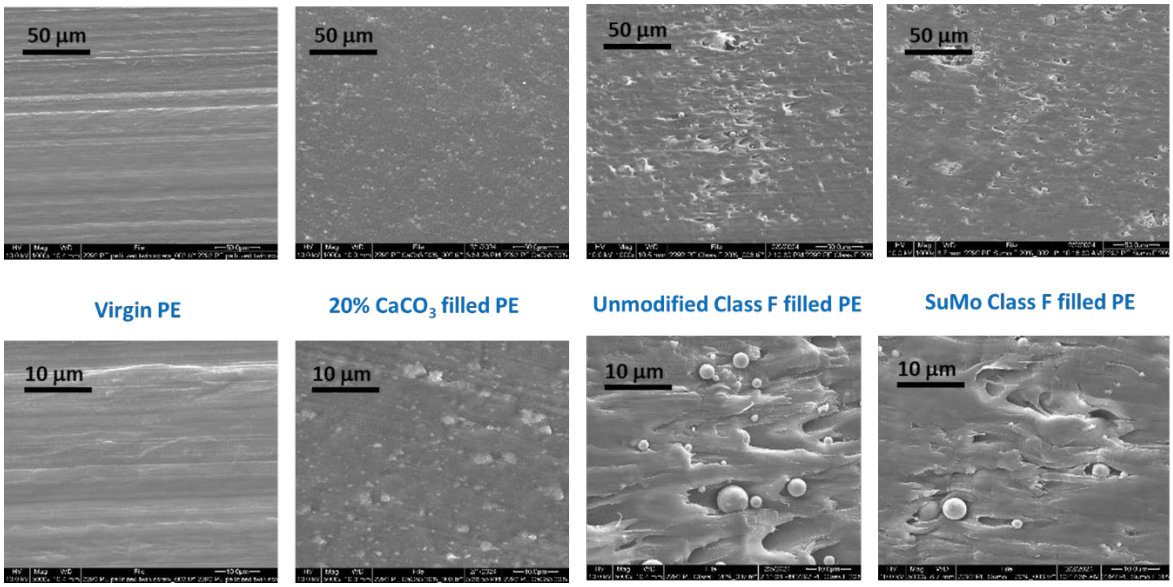

***Figure 23**. SEM images of unmodified Class F, SuMo Class F and $CaCO_3$ incorporated PE thermoplastics*

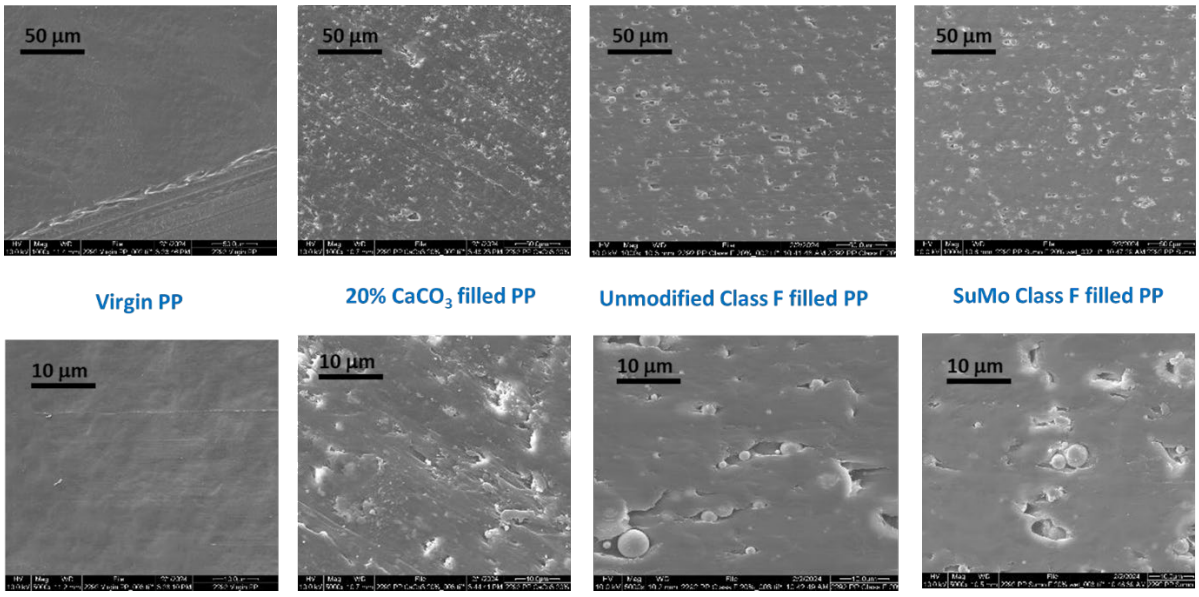

Figure 24. *SEM images of unmodified Class F, SuMo Class F and $CaCO_3$ incorporated PP thermoplastics*

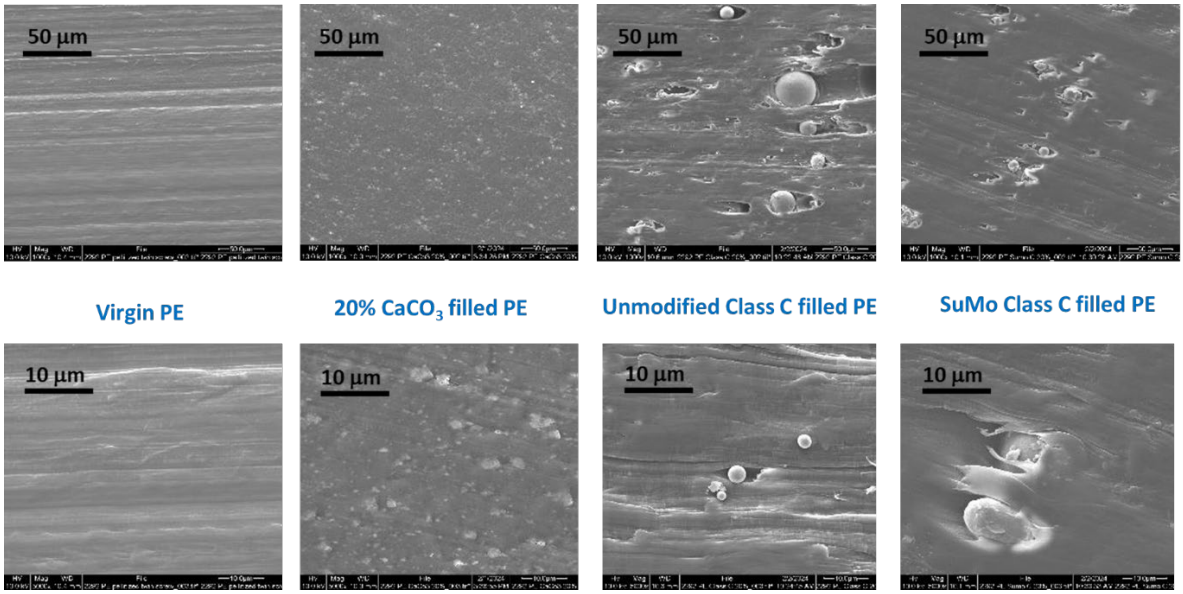

Figure 25. *SEM images of unmodified Class C, SuMo Class C and $CaCO_3$ incorporated PE thermoplastics*

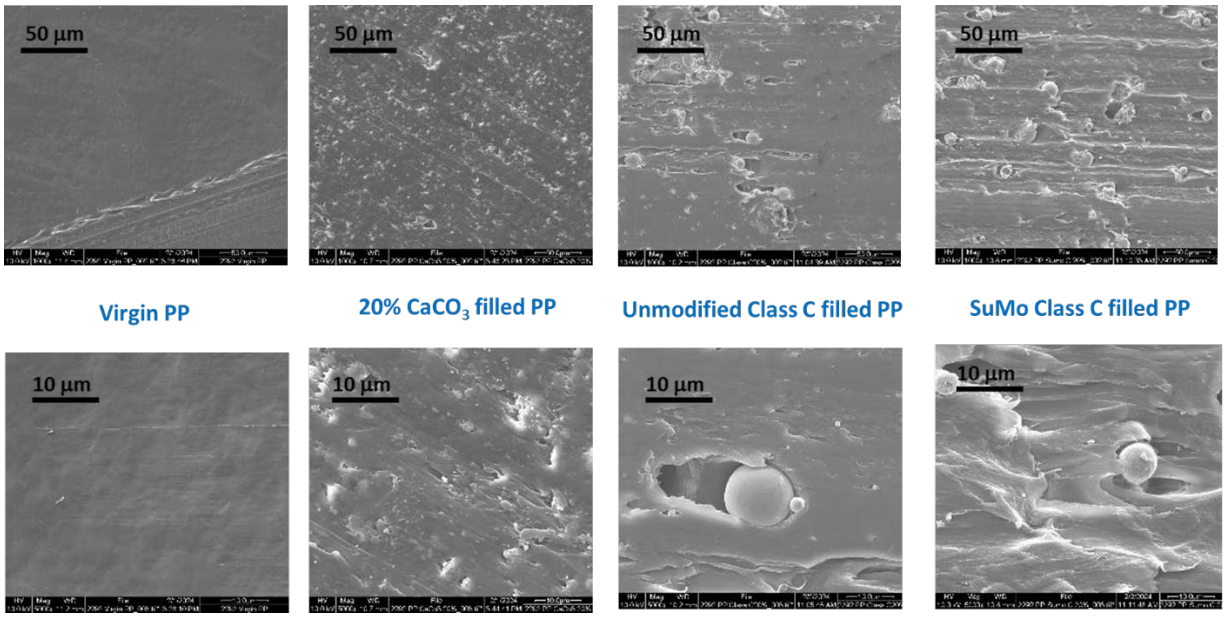

***Figure 26**. SEM images of unmodified Class C, SuMo Class C and $CaCO_3$ incorporated PP Thermoplastics*

The thermal degradation of the virgin polymers PP, PE as well as the filler-based thermoplastics (PP + $CaCO_3$, PP + fly ash, PP + SuMo fly ash, PE + $CaCO_3$, PE + fly ash and PE + SuMo fly ash) are shown in ***Figures 27-28***. The onset temperature for virgin PP polymer was 304ºC. Among the PP test bars, SuMo fly ash-filled thermoplastics had the highest onset temperature of 389ºC (SuMo class F) and 410ºC (SuMo class C) conforming to a higher thermal stability. It indicates that surface modification of fly ash synergistically enhances the thermal stability of thermoplastics. In the case of PE, TGA trends for all thermoplastics were overall similar. The onset temperature for virgin PE and unmodified fly ash filled PE thermoplastics was close to 412ºC. The SuMo fly ash filled PE polymer has an onset temperature of 430ºC which conforms to the ones observed for $CaCO_3$ filled PE thermoplastics.

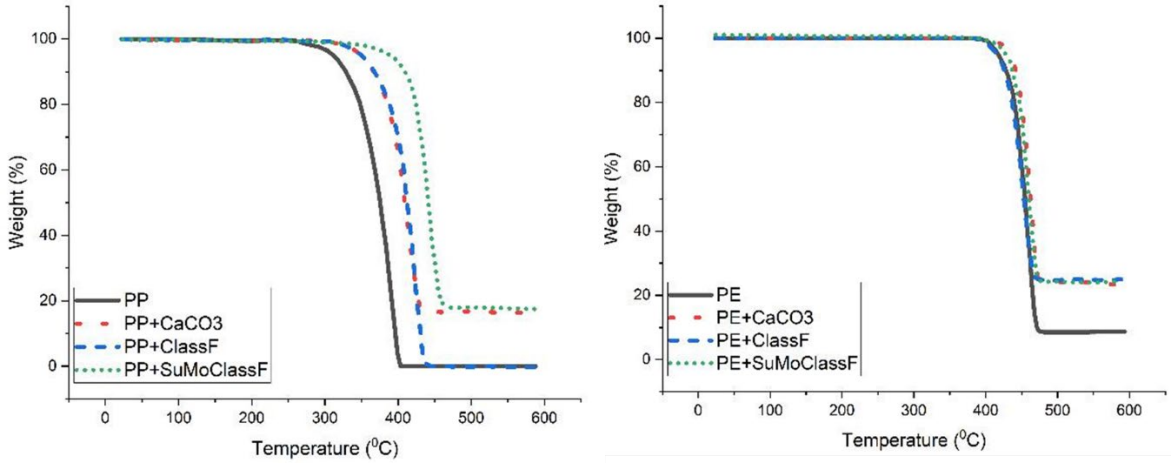

***Figure 27**. Thermal stability of unmodified Class F, SuMo Class F and $CaCO_3$ incorporated PE and PP thermoplastics*

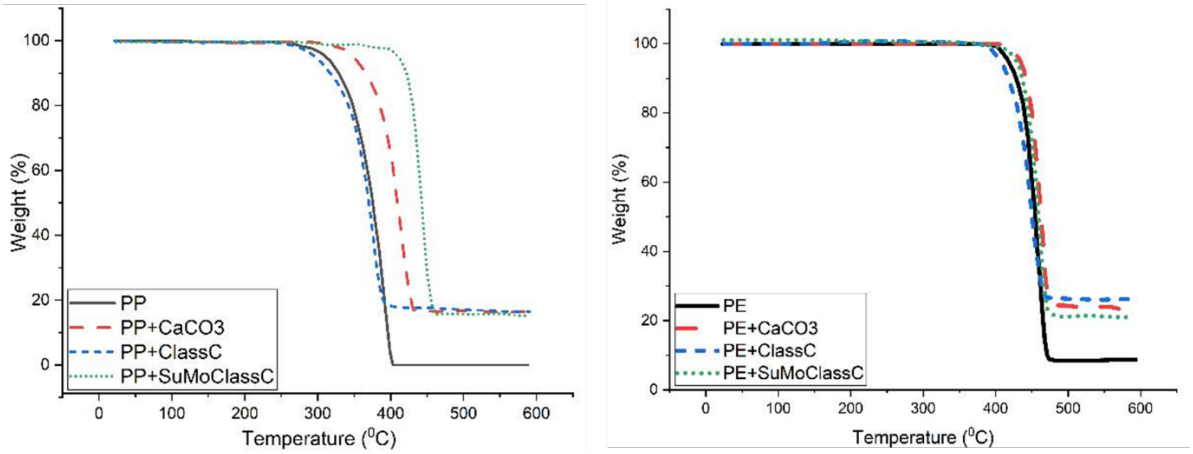

***Figure 28**. Thermal stability of unmodified Class C, SuMo Class C and $CaCO_3$ incorporated PE and PP thermoplastics*

The tensile test specimens were evaluated for tensile strength, tensile modulus, and elongation at break using a mechanical wedge action grip accessory on an Instron as per **ASTM D638**. The flexural testing (strength and modulus) was performed using a three-point bending fixture on an Instron according to **ASTM D790**. The thermoplastics are given nomenclature in the form (Compounding polymer + Filler type).

Figures 29-32 present the mechanical material properties of the compounded thermoplastics in terms of modulus (in tensile and flexural straining) and strength (at yield and ultimate). In the case of PE based thermoplastics, SuMo fly ash as fillers reduced the stiffness in flexural loading and increased in tensile loading (Class F) (***Figure 29***). A similar increase of 40% in tensile modulus for silane treated fly ash at (30% addition by volume in HDPE) was reported by ***Deepthi et al. (2010)***. The incorporation of SuMo fly ash as fillers increased the tensile yield strength of

PE and reduced the ultimate strength. This decrease in ultimate strength was consistent for all filler types, which would imply that the ultimate strength was largely governed by the PE content.

The stiffness of PP + SuMo fly ash was lower than that of PP + fly ash predominantly because of the coating being rubbery in nature. Nevertheless, at the same percentage of silane treated fly ash filler in PP resulted in an increase in tensile modulus by 27% ***(Das et al., 2011)***, which was like that of SuMo fly ash (by 24%). The yield strength of PP + SuMo fly ash was the highest among all the thermoplastics. The yield strength for PP + SuMo fly ash thermoplastics exhibited an increase of 97% compared to unfilled PP thermoplastics (***Figure 30***). This indicates that under working conditions, the material strength was enhanced by SuMo fly ash incorporation. Moreover, the ultimate strength of SuMo fly ash-based PP thermoplastics was found to be exactly as that of $CaCO_3$ based PP thermoplastics. PP incorporated with 5% weight of fly ash modified by carboxymethyl cellulose (CMC) and cetyltrimethylammonium bromide (CTAB) treatment resulted in an increase in tensile strength by 7-13% ***(Maurya et al., 2021)***.

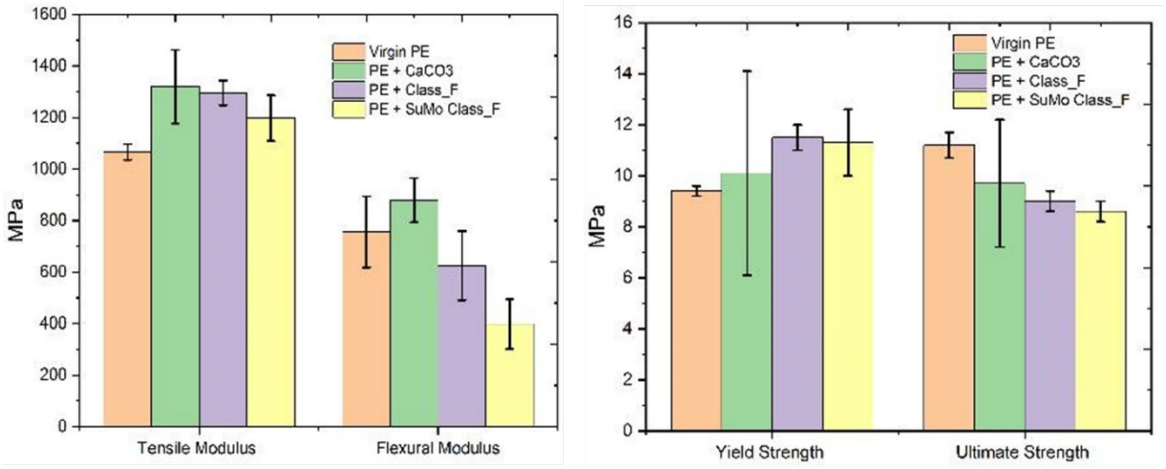

Figure 29. *Modulus and Strength of unmodified Class F, SuMo Class F and $CaCO_3$ incorporated PE*

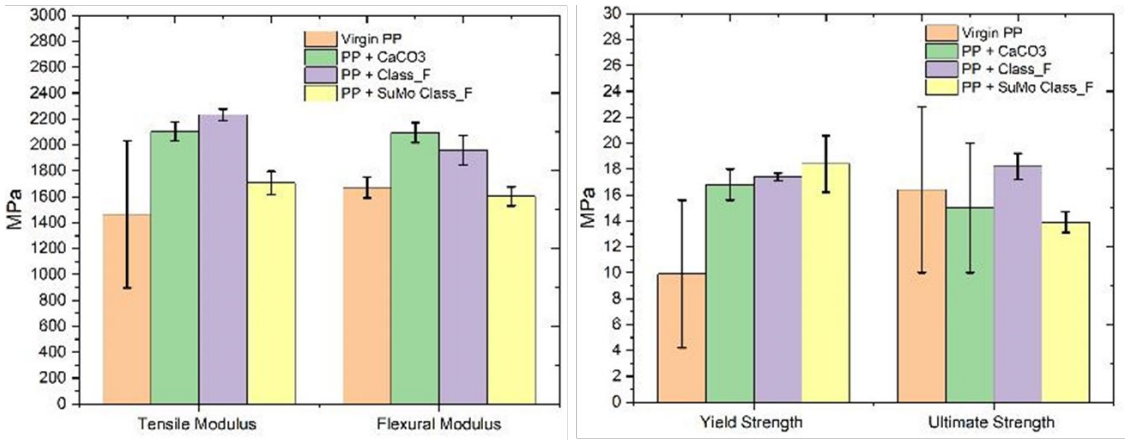

***Figure 30**. Modulus and Strength of unmodified Class F, SuMo Class F and $CaCO_3$ incorporated PP*

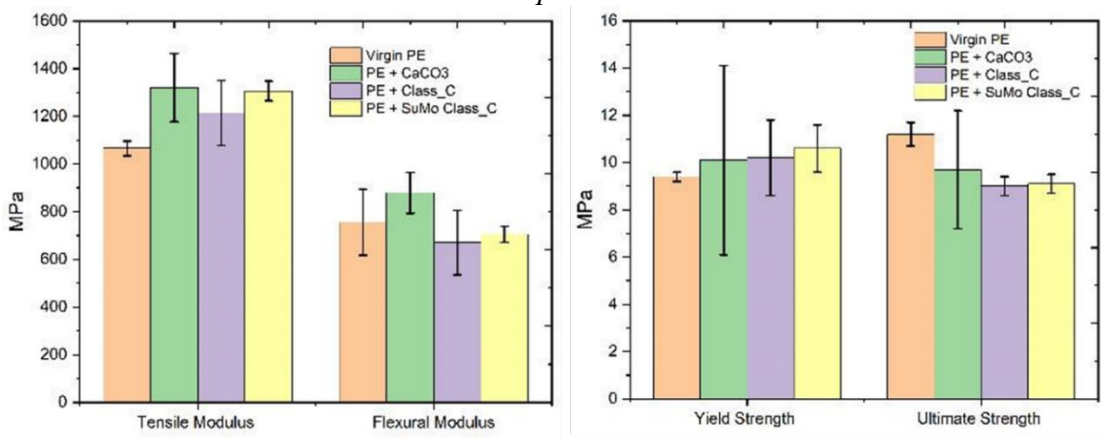

***Figure 31**. Modulus and Strength of unmodified Class C, SuMo Class C and $CaCO_3$ incorporated PE*

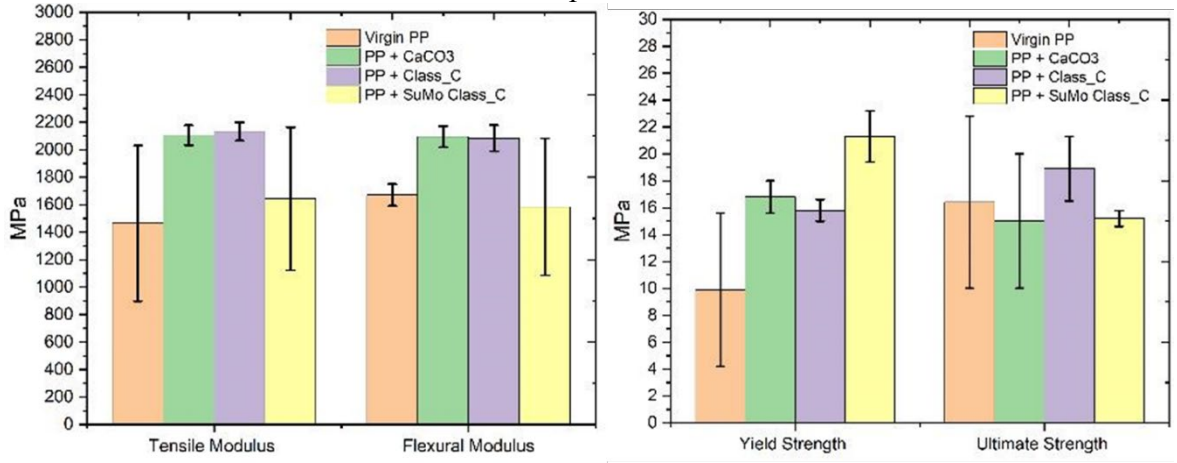

***Figure 32**. Modulus and Strength of unmodified Class C, SuMo Class C and $CaCO_3$ incorporated PP*

The ductility in terms of elongation at break reduced in PE and increased in PP (except SuMo Class C) for all filler type (***Figures 33-34***). The rubbery polymer coating would be able to dissipate strains without readily breaking. In literature (***Sengupta et al., 2013***), application of palmitic acid or silane coupling agents to surface modify fly ash did not improve the ductility of PP, rather resulted in brittle nature up to an application rate of 5% by weight.

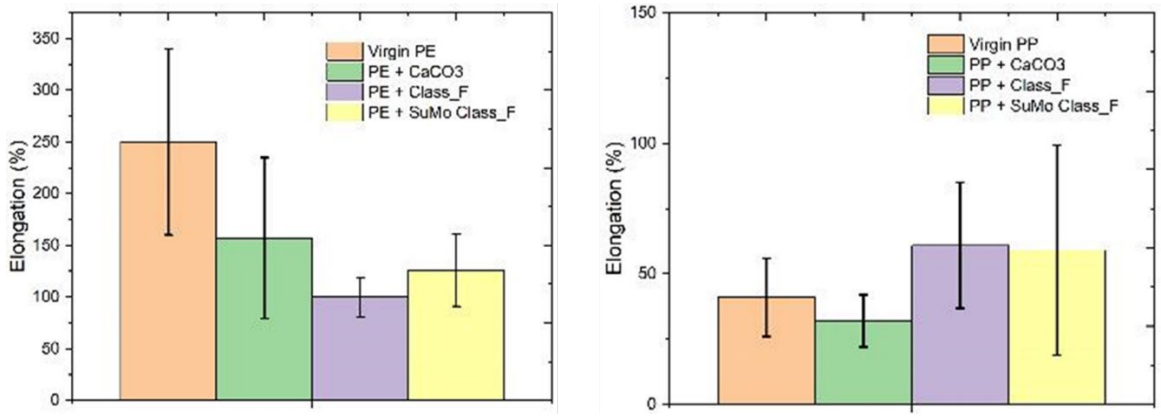

Figure 33. *% Elongation of unmodified Class F, SuMo Class F and $CaCO_3$ incorporated PE and PP*

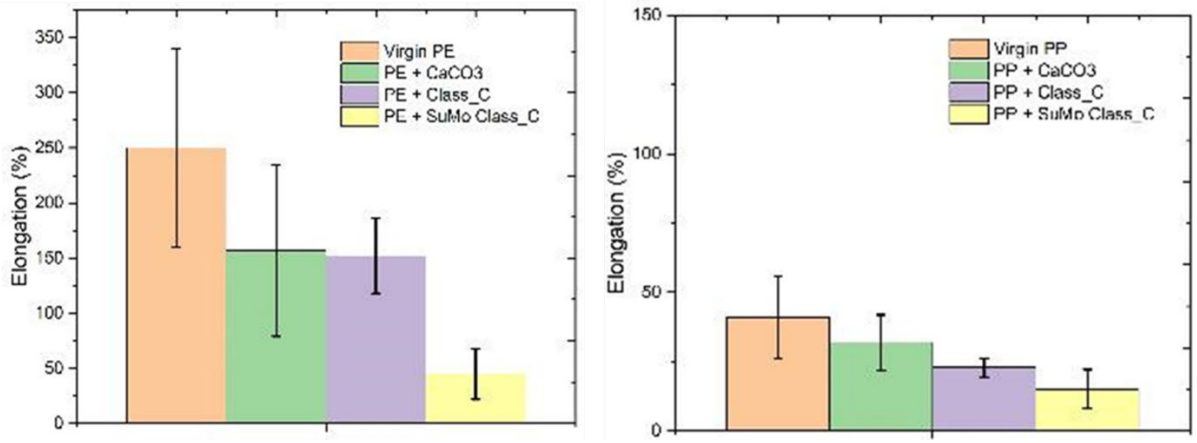

Figure 34. *% Elongation of unmodified Class C, SuMo Class C and $CaCO_3$ incorporated PE and PP*

Figures 35-36 present the notch and not-notched impact strength of tested PE and PP thermoplastics with and without fillers. It was evident that not-notched PE thermoplastics generally improved for all filler types with no breakage observed. This means that most of the energy was dissipated majorly by the PE thermoplastics and incorporation of fillers had mild changes in energy absorption. However, notch impact strength was reduced by at least 40% for filler filled thermoplastics. In the case of fly ash-based filler, both fly ash and SuMo fly ash exhibited no appreciable change in notched strength (***Figure 35***). However, the dispersity reduced

considerably for SuMo fly ash-based PE thermoplastics. Maleic anhydride treated fly ash (at 10% filler application) coupled with natural banana fiber inclusion (at 3%) resultant in a decrease in impact strength by 77% (***Satapathy and Kothapalli, 2018***). In general, it showcases that filler application in PE reduces the energy absorption capacity of the compounded thermoplastics. In the case of $CaCO_3$ filled PP thermoplastics, the impact strength for both notched and not-notched samples were lower than that of pure PP thermoplastics with complete failure. In actual product design, the notch effect (stress concentration) often cannot be avoided due to shape of the product and other factors. Thus, the notched impact strength of thermoplastics is generally viewed as more important. The highest notch impact strength was observed for SuMo fly ash filled PP with a 25% increase with respect to pure PP. Palmitic acid treated fly ash in PP at 5% (by weight) filler application rate resultant in a decrease in impact strength by 45% (***Sengupta et al., 2013***). In comparison to fly ash, the SuMo fly ash exhibited better dispersity (based on variability) within the PP matrix.

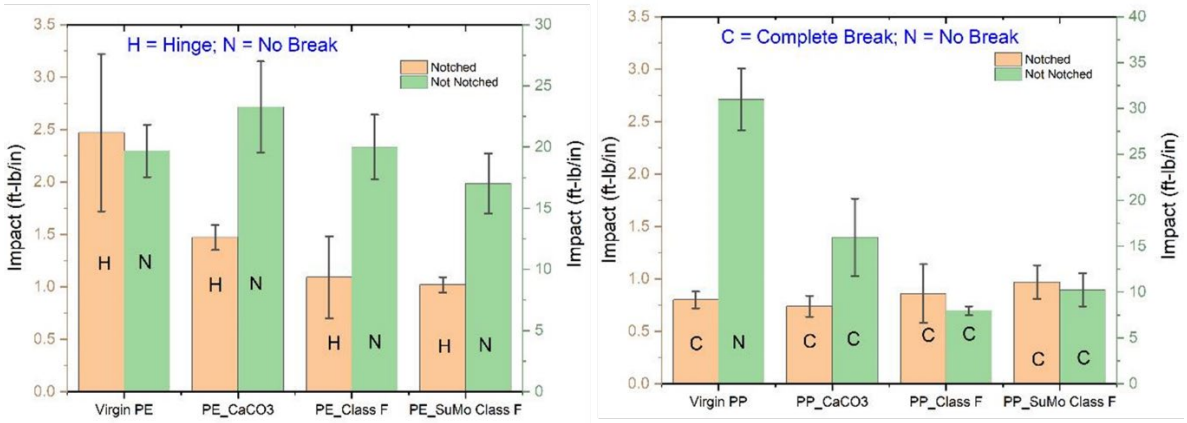

Figure 35. *Impact testing strengths of unmodified Class F, SuMo Class F and $CaCO_3$ incorporated PE and PP*

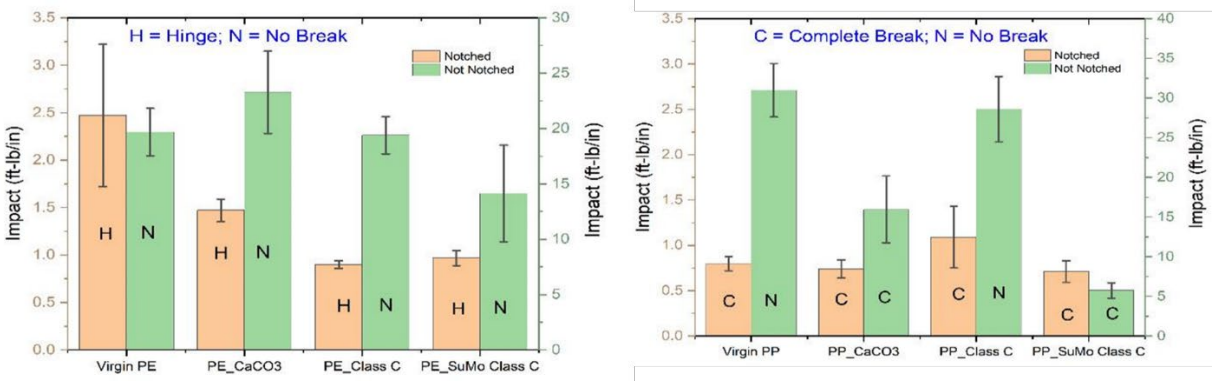

Figure 36. *Impact testing strengths of unmodified Class C, SuMo Class C and $CaCO_3$-incorporated PE and PP*

4.2 Replacement of Carbon Black Filler in Crosslinked Rubbers

Many Hevea natural rubber-based (HNR) vulcanized products are reinforced by carbon black (CB) or silica fillers (***Salaeh and Nakason, 2012***; ***Barana et al, 2019***) to attain needed mechanical properties (***Fan et al., 2020***). Diluent non-reinforcing fillers, such as clay and calcium carbonate, are also used to lower the overall material cost but often reduce mechanical performance.

In the past decade, substitute fillers for CB in rubber compounds have been explored. They included eggshell, limestone dust, peanut shell powder, rice husk and fly ash (***Barrera and Cornish, 2016, 2019, 2022***; ***Barrera et al., 2018***; ***Fan et al., 2020***; ***Ren and Cornish, 2019***). Among them, fly ash (FA) is abundantly available in most developing countries and exists as legacy waste in developed countries. FA particles are suitably sized for use as rubber filler, are spherically shaped like carbon black, and FA composites have similar stiffness to CB composites (***Sombatsompop et al., 2004***; ***Thongsang and Sombatsompop, 2005***; ***Ren and Sancaktar, 2019***).

Hevea (Technical Specified Rubber TSR-10) conforming to ASTM D7050-04 (2019) was obtained from Hexpol Pvt. Ltd (Middlefield, OH). Compounding chemicals and carbon black-N234 (mean particle size: 2μm) were also procured from Hexpol.

The compounding process of fillers in Hevea NR-based elastomers adopted in this study has been described (***Barrera and Cornish, 2016***; ***Ren et al., 2020***). A total filler loading of 50phr (parts per hundred rubber) was selected for the compounding process. A total of 14 different natural rubber composites were made. The detailed composition and additives used to compound are shown in ***Tables 9*** and ***10***. A two-step mixing procedure was employed by Hexpol to ensure that all ingredients were dispersed thoroughly in the compound. In the first (non-productive) step, the NR and mixer were warmed by first masticating HNR alone for 2 minutes; half portions of the CB and FA or SuMo were added and mixed for 3 minutes; this was followed by addition of naphthenic oil and the other half of the CB and FA or SuMo. Then 6PPD, ZnO and stearic acid (in compounds where SuMo FA was not used) were added and mixed at 30 rpm for 60 sec using an internal mixer at Hexpol (Burton, OH). The sulfur and TBBS were then added and mixed for 2 minutes to initiate the vulcanization process. These mixtures were dumped, and the mix temperature recorded. The mixtures were then processed on a two-roll mill for 5-7 passes to further mix the compounds. The samples were later cured in a mold at 160°C for 12 minutes on a heated press (Rubber City Machinery, Akron, OH) under 16 metric tons of pressure according to ASTM D3182. The resulting 3mm thick rubber sheets were used for materials testing. Hexpol conducted

the testing for Shore A hardness, ultimate tensile stress, and ultimate elongation on-site. Crosslink density of the compounded elastomers was calculated from swelling data using the Flory-Rehner and Kraus equations and compared with CLD obtained from tensile data using the Mooney-Rivlin equation.

Statistical analyses were conducted on each measured parameter to assess the significance level of effects two-way analysis of variance (ANOVA) for estimating statistical significance level values. A significance value of p <0.05 was used as a measurement of statistically significant differences. Mean values were plotted for the majority of the measured properties.

Table 9. *Detailed composition of the elastomer composites*

Ingredient	Control	5 wt% Fly Ash + 95 wt% Carbon Black	10 wt% Fly Ash + 90 wt% Carbon Black	20 wt% Fly Ash + 80 wt% Carbon Black	40 wt% Fly Ash + 60 wt% Carbon Black
Wt% of Fly Ash with respect to the total weight of the filler	0	5	10	20	40
PHR Fly Ash	0	2.5	5	10	20
Wt% of Carbon Black N234 with respect to the total weight of the filler	100	95	90	80	60
PHR Carbon Black	50	47.5	45	40	30
Total PHR amount of Fly Ash + Carbon Black N234	50	50	50	50	50
PHR **Hevea** natural rubber	100	100	100	100	100
PHR Naphthenic Oil	20	20	20	20	20
PHR ZnO	5	5	5	5	5
PHR Stearic Acid	1	1	1	1	1
PHR 6PPD	2	2	2	2	2
PHR Sulfur	4.5	4.5	4.5	4.5	4.5
PHR TBBS	1	1	1	1	1

Table 10*. High-level composition of the fourteen elastomer composites*

Class C Fly Ash - Modified (SuMo)	Class F Fly Ash - Modified (SuMo)	Class F Fly Ash - Unmodified
0 wt% Fly Ash + 100 wt% Carbon Black 0 PHR Fly Ash + 50 PHR Carbon Black	0 wt% Fly Ash + 100 wt% Carbon Black 0 PHR Fly Ash + 50 PHR Carbon Black	0 wt% Fly Ash + 100 wt% Carbon Black 0 PHR Fly Ash + 50 PHR Carbon Black
5 wt% Fly Ash + 95 wt% Carbon Black 2.5 PHR Fly Ash + 47.5 PHR Carbon Black	5 wt% Fly Ash + 95 wt% Carbon Black 2.5 PHR Fly Ash + 47.5 PHR Carbon Black	**HAS NOT BEEN CREATED**
10 wt% Fly Ash + 90 wt% Carbon Black 5 PHR Fly Ash + 45 PHR Carbon Black	10 wt% Fly Ash + 90 wt% Carbon Black 5 PHR Fly Ash + 45 PHR Carbon Black	10 wt% Fly Ash + 90 wt% Carbon Black 5 PHR Fly Ash + 45 PHR Carbon Black
20 wt% Fly Ash + 80 wt% Carbon Black 10 PHR Fly Ash + 40 PHR Carbon Black	20 wt% Fly Ash + 80 wt% Carbon Black 10 PHR Fly Ash + 40 PHR Carbon Black	20 wt% Fly Ash + 80 wt% Carbon Black 10 PHR Fly Ash + 40 PHR Carbon Black
40 wt% Fly Ash + 60 wt% Carbon Black 20 PHR Fly Ash + 30 PHR Carbon Black	40 wt% Fly Ash + 60 wt% Carbon Black 20 PHR Fly Ash + 30 PHR Carbon Black	40 wt% Fly Ash + 60 wt% Carbon Black 20 PHR Fly Ash + 30 PHR Carbon Black

The ESEM micrographs of tear surfaces of cured NR compounds indicated that the 100% CB control was quite homogeneous and that the CB particles appeared attached to the rubber matrix

(***Figures 37-38***). Unmodified fly ash did not fully incorporate into composites (not well dispersed). The SuMo fly ash particles were well dispersed with no agglomeration.

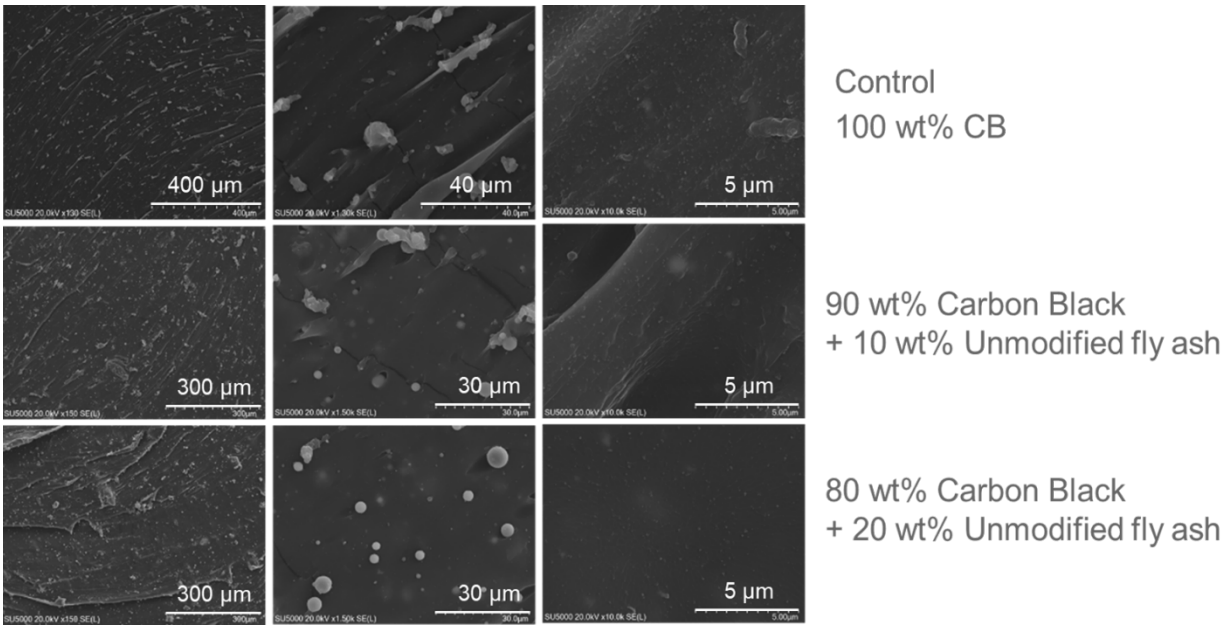

Figure 37*. ESEM images of unmodified Class F and CB incorporated elastomers*

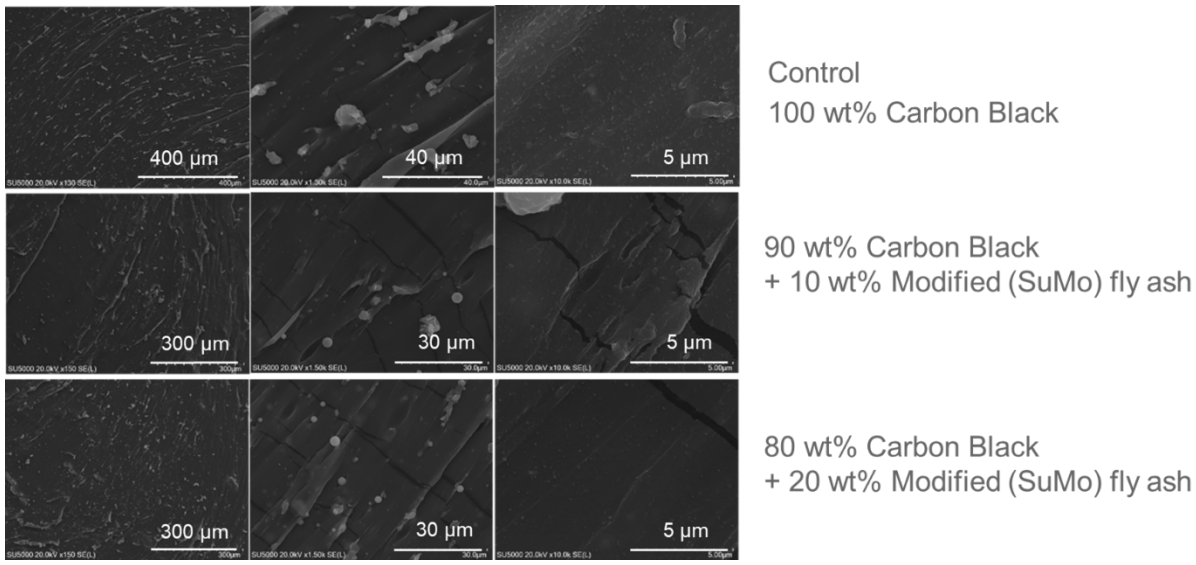

***Figure 38**. ESEM images of SuMo Class F and CB incorporated elastomers*

Figures 39-41 show the stress-strain plot for uncoated Class F, SuMo Class F, and SuMo Class C incorporated elastomers. For uncoated Class F incorporated elastomers, tensile strength decreased as ash wt% increased, elongation to break was similar among all samples, 10 wt% may be an acceptable replacement level (***Figure 39***). For SuMo Class F incorporated elastomers, tensile stress at break was reduced by 10 wt% and 20 wt% SuMo fly ash than by unmodified fly ash (***Figure 40***). Sumo Class C fly ash gave similar results to SuMo Class F fly ash. Surface modifications allow more fly ash to be added to the composites (up to 20 wt%) than possible with unmodified fly ash (10 wt%) (***Figure 41***).

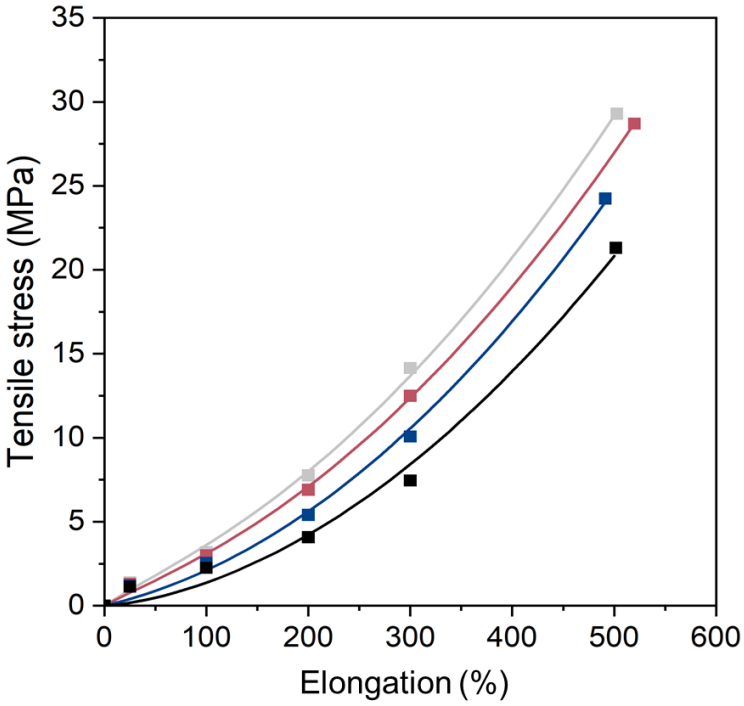

Figure 39. *Stress-strain Plots of Compounds Containing unmodified Class F fly ash*

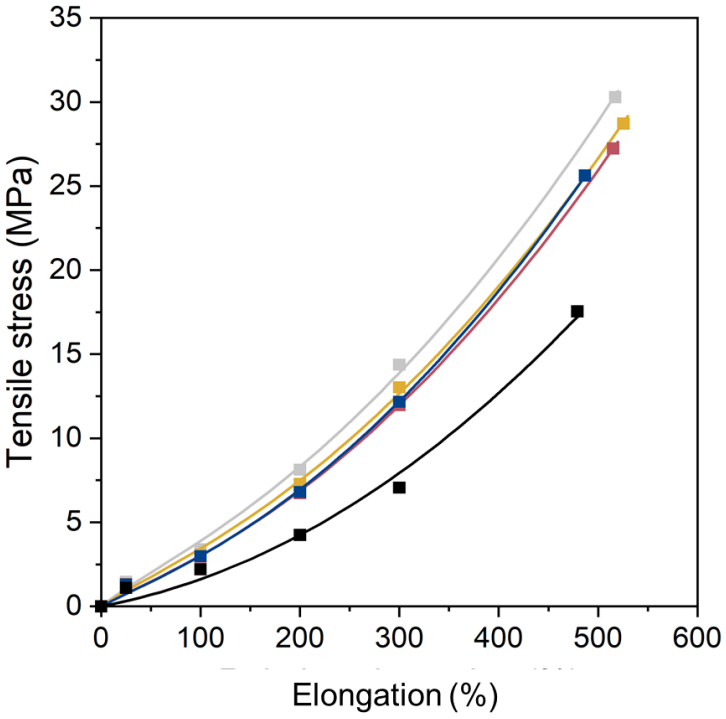

Figure 40. *Stress-strain Plots of Compounds Containing SuMo Class F fly ash*

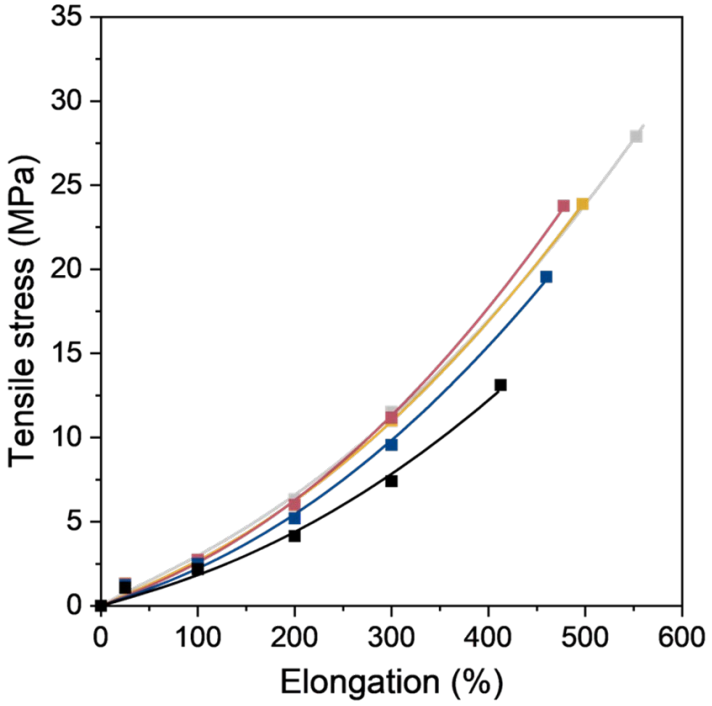

Figure 41. *Stress-strain Plots of Compounds Containing SuMo Class C fly ash*

The crosslink density plot is shown in ***Figure 42***. Chemical crosslink densities (CLD) were calculated from swelling data using the Flory-Rehner equation. Crosslink density declined with replacement of carbon black by modified fly ash composites. Both SuMo fly ash-maintained crosslink density up to 20wt% carbon black replacement.

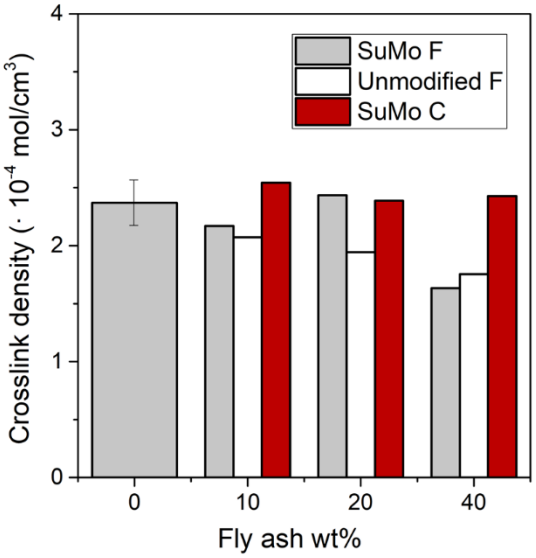

Figure 42. *Crosslink Densities of Compounds Containing fly ash*

The shore hardness plot is depicted in ***Figure 43***. Shore hardness declined as the amount of fly ash increased. SuMo Class F composite maintained hardness the best up to 20 wt% replacement.

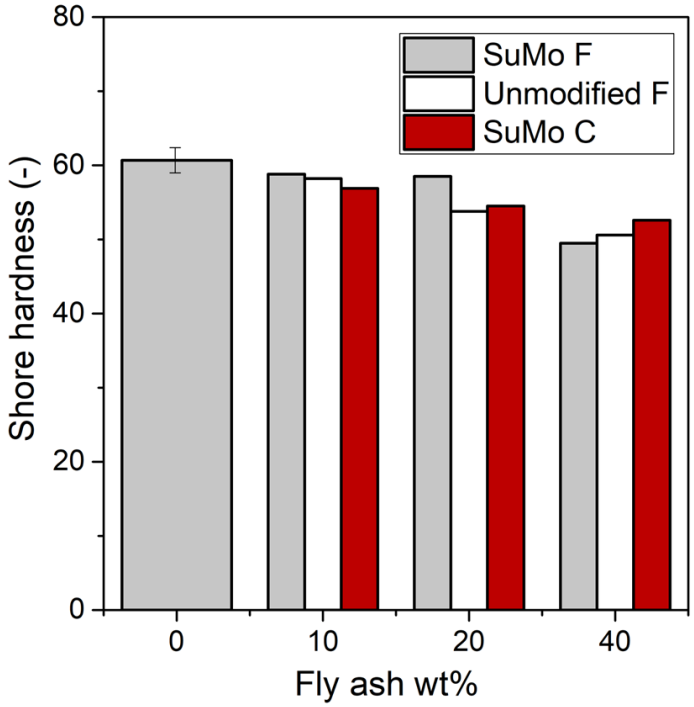

Figure 43. *Shore Hardness of Compounds Containing fly ash*

See ***Table 11*** for the glass transition temperature results for the unmodified Class F, SuMo Class F and SuMo Class C fly ash elastomer composites. It demonstrates that the incorporation of fly ash (unmodified or modified) has no significant impact on the glass transition temperature.

Table 11. *Glass Transition Temperature of elastomer composites*

	Glass Transition Temperature (°C)		
Composition of the filler	**Class F Unmodified Fly Ash**	**Class F Modified Fly Ash**	**Class C Modified Fly Ash**
0 wt% Fly Ash + 100 wt% Carbon Black	-58.2 ± 0.6	-58.2 ± 0.6	-58.2 ± 0.6
10 wt% Fly Ash + 90 wt% Carbon Black	-58.0	-59.0	-59.3
20 wt% Fly Ash + 80 wt% Carbon Black	-58.1	-58.1	-60.0
40 wt% Fly Ash + 60 wt% Carbon Black	-57.3	-57.4	-59.3

Surface modification of the Fly Ash did not affect the glass transition temperature.

5. ENVIRONMENTAL CHARACTERIZATION OF SUMO FLY ASH AND FINAL PRODUCTS

The SuMo Fly Ash and the upcycled (surface coated) elastomers and plastics were ground for screening-level and leaching assessment of a series of following inorganic constituents of potential concern (COPC), including mercury (Hg), arsenic (As), cadmium (Cd), chromium (Cr), boron (B), lead (Pb), and selenium (Se).

5.1 Leaching

The surface modification approach was applied, SuMo, as a method to reduce the leachability of hazardous components of fly ash and thus increasing its potential as filler in high-value applications in various industries. SuMo features a sustainable and water-repellent polysulfide polymer coating on fly ash surface, produced by inverse vulcanization, wherein waste sulfur and waste oil derivatives are reacted near their melting points (***Chalker et al., 2019***). This study evaluates the leachability of this eco-friendly and hydrophobic fly ash under variable pH conditions.

Uncoated and synthesized SuMo particles (subtask 3.3) and ground upcycled products were probed as per the Leaching Environmental Assessment Framework. The tests allow the determination of leaching of metals and COPC under a wide range of environmentally relevant conditions such as pH (Method 1313). Method 1313 allowed the comparison of the leaching potential of uncoated (control) and hydrophobically coated SuMo fly ash as well as the determination of the effectiveness of the coating methods (subtasks 3.1/3.2). Finally, the leaching potential of end-of-life materials were determined using finely ground SuMo-incorporated plastics/elastomers using Method 1313.

As pH conditions have been identified as a crucial factor influencing elemental species and leaching extent in fly ash, pH-dependent leaching tests were conducted following the Leaching Environmental Assessment Framework (LEAF) methods established by the United States Environmental Protection Agency (EPA). The selected fly ash samples were randomly mixed from different containers to account for potential variability arising from distinct production batches. Prior to initiating any leaching assessment studies, laboratory utensils were cleaned with ethanol, rinsed with deionized (DI) water, and then dried in a furnace. All batch leaching tests were conducted at an L:S ratio of 10mL/g unless described otherwise. Varied aliquots of 2M nitric acid (HNO_3) or 1M potassium hydroxide (KOH) were added to containers to suspend fly ash and to

achieve the desired endpoint pH. The fly ash suspension samples were then thoroughly mixed using an orbital shaker at a speed of 100±20 rpm over a 24-hour period.

When harvesting samples, the fly ash suspension samples were allowed to settle, and the supernatant was filtered through a 0.2µm membrane filter. From each extraction, a portion of the filtrate sample was collected for the measurement of pH, oxidation–reduction potential (ORP), and electrical conductivity (EC), serving as quick indicators of leaching extents. EC was considered as an initial gauge of leaching extents due to its correlation with the amount of ions/cations in water. Additionally, pH measurements could assess the leaching of CaO from fly ash ***(Khosla et al., 1979)***. EC was determined using the Oakton™ CON 6+ Portable Conductivity Meter, while pH measurements were performed using the PH700 Benchtop pH Meter Kit. The remaining filtrate samples were stored in trace element-free falcon tubes at 4°C for subsequent elemental analysis. To minimize interference from any organic matter and convert leached metals into free metal forms, all filtrate samples underwent digestion following the EPA Methods 3010. Elemental analysis was conducted using a Varian Vista-MPX Ion Coupled Plasma-Optical Emission Spectrometry (ICP-OES) system.

To evaluate the effectiveness of SuMo in reducing the leaching potential of fly ash, leaching experiments were conducted with coated Micron^3 samples under pH 4-12, and the results were compared with those of uncoated samples. SuMo fly ash exhibited a stronger acid neutralization capacity (ANC) compared to the uncoated sample (***Figure 44A***). The natural eluate of the uncoated fly ash suspension with deionized (DI) water was alkaline as indicated by equation **(1)**, showing a pH of 11.8 with no acid addition (open circle in ***Figure 44A***). This alkalinity, contributed by carbonate species in fly ash (***Table 4***), imparts a pH buffering capacity or ANC (***Komonweeraket et al., 2015***). With acid addition ranging from 0.3meq/g to 13meq/g, the eluate pH of uncoated fly ash slowly decreased from pH 10.2 to pH 2.3 due to carbonate neutralization. In comparison, the pH of the natural eluate of SuMo fly ash was 9.1 (open star in ***Figure 44A***), lower than that of the uncoated fly ash leachate. With the same acid addition as the uncoated sample, the pH of SuMo fly ash suspension dropped from 8.3 to 2, indicating a higher concentration of H^+ compared to the uncoated sample. The acid addition altered eluate pH of coated sample more efficiently because of lack presence of OH^- due to a reduced interaction between fly ash component, i.e., carbonate oxide, and water (based on ***equation 1***).

$$CaO + H_2O \rightarrow Ca^{2+} + 2OH^- \qquad \textbf{(1)}$$

Besides the leaching process, leachate pH was also a crucial factor influencing oxidation-reduction condition (ORP) of the leachate. Positive ORP values, indicative of oxidizing conditions, were associated with acidic conditions. Consistent with other studies (***Zhang et al., 2016***), the eluate ORP of both samples exhibited a linear decrease with increasing pH, attaining a reducing

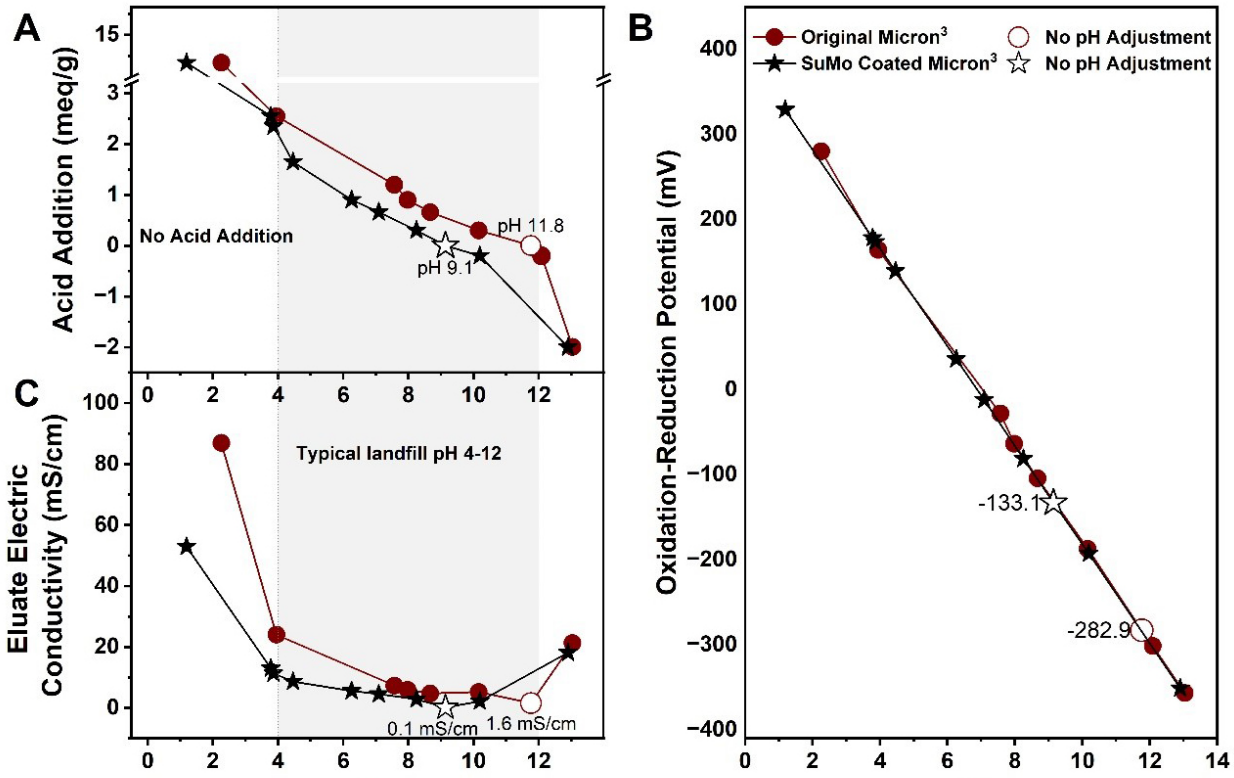

Figure 44*. pH and electric conductivity (EC) behavior of fly ash leaching suspension:* ***A)*** *acid neutralization capacity (ANC) curve,* ***B)*** *pH-dependent oxidation-reduction potential (ORP), and* ***C)*** *pH-dependent eluate EC for uncoated and SuMo-coated Micron³ fly ash. The open symbols refer to the eluate pH, EC, and ORP readings of leaching samples with no acid or base addition*

condition under alkaline conditions (***Figure 44B***). Importantly, coating did not alter the relationship between eluate pH and ORP.

The pH-dependent eluate electrical conductivity (EC) serves as a rapid measurement of leaching potential of fly ash, as leachate EC is influenced by the amount of diffused elements. As depicted in ***Figure 44C***, when plotting eluate EC against pH, both original and coated samples exhibited slight variations within the range of 1.6-24 mS/cm at eluate pH 4.0-11.8. Both eluate EC increased at extreme acidic conditions, reaching 86.9 and 52.9mS/cm, and at alkaline conditions, reaching 21.2 and 18.1mS/cm, respectively, indicative of enhanced leaching conditions. Importantly, the EC-pH curve of the original fly ash consistently remained above that of the SuMo

sample (***Figure 44C***). This implies that for eluate samples with the same pH (or the same H^+ concentration), the leachate from the latter sample had a lower ionic strength due to fewer diffused elements. As EC is considered non-specific and does not measure any unique species, the leaching behavior of coated and original Micron^3 samples was further characterized by examining various elements of potential concern in the eluate.

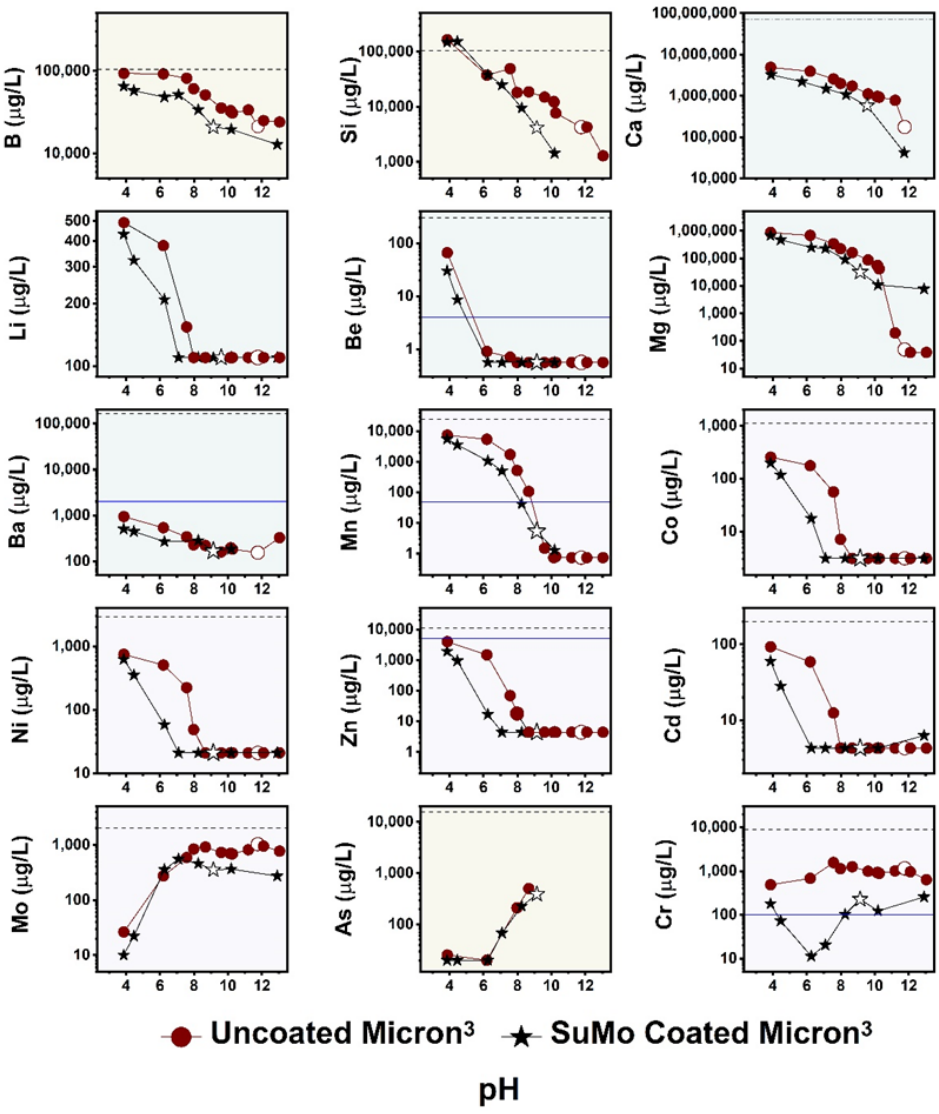

Figure 45. *pH-dependent elemental concentration of leachate of original and SuMo coated fly ash for elements that follow a cationic pattern. The eluate concentrations of uncoated and coated samples are indicated by solid red circle and black star symbols, respectively, except the data at their own pH are shown by open symbols. The black dash line indicates the possible maximum elemental concentration calculated based on their total content on fly ash, and the blue line indicates the maximum contaminant level in drinking water regulated by EPA.*

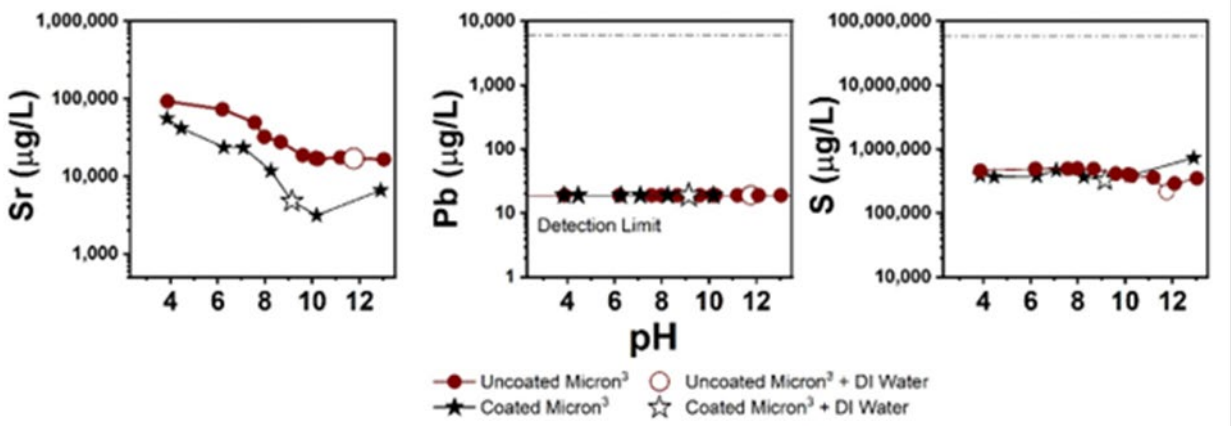

Figure 46. *pH-dependent elemental concentration of leachate of original and SuMo-coated fly ash for Strontium, Lead, and Sulfur. The eluate concentrations of uncoated- and coated-samples are indicated by solid red circle and black star symbols, respectively, except the data at their own pH are shown by open symbols. The black dash line indicates the possible maximum elemental concentration calculated based on their total content on fly ash*

The leaching experiment examined alkali/alkaline earth metals, transition metals, and metalloids, each with diverse elemental properties. The pH-dependent liquid-to-solid partitioning (LSP) behaviors of the elements revealed three main patterns (***Figure 45*** and ***Figure 46***): (i) a cationic pattern for B, Ba, Be, Ca, Cd, Co, Li, Mg, Mn, Ni, Si, Sr, and Zn, where eluate concentration decreases monotonically with increasing pH; (ii) an oxyanionic pattern for As and Mo, with eluate concentration increasing under alkaline conditions; and (iii) an amphoteric pattern for Cr leaching from coated fly ash samples.

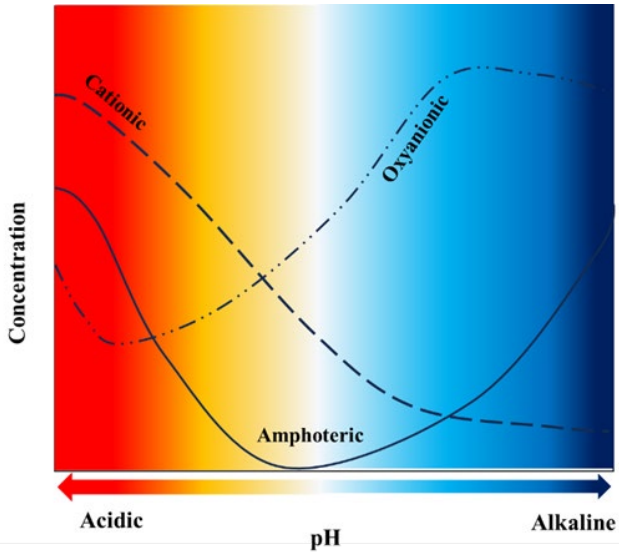

Figure 47. *Three types of leaching pattern as a function of pH. (Modified after* ***Komonweeraket et al., 2015****)*

A conceptual illustration of these pH-dependent leaching patterns is provided in ***Figure 47***. Additionally, S, Hg, and Cr (from the uncoated sample) showed constant levels of leaching across the entire pH range. The observed pH-dependent leaching patterns were ascribed to the speciation of the leached elements, influenced by processes such as precipitation, complexation, exchange mechanisms, crystallization, and redox potential.

Boron (B), known for its high leaching potential due to surface association, demonstrated up to 65% leaching in previous studies (***Cox et al., 1978***; ***James et al., 1982***; ***Sear et al., 2003***; ***Ward et al., 2003***). In this investigation, the leachate concentration of B at the natural pH (pH 11.8) of the uncoated sample was 21,166µg/L, indicating 20% of B in Micron^3 was water-extractable (***Figure 45***). As the leachate pH decreased to pH 10, 7, and 4, B in leachate rose to 33,079µg/L, 81,489µg/L, and 93,534µg/L, respectively, equivalenting 32, 78, and 90% of total B being mobilized. This cationic leaching pattern of B was also observed in previous studies (***Cox et al., 1978***; ***Iwashita et al., 2005***, ***Zhao et al., 2020***), and was attributed to ligand exchange mechanisms and coprecipitation with $CaCO_3$ under alkaline conditions (***Mahasti et al., 2022***). For SuMo Micron^3, the LSP of B as a function of pH also followed a cationic pattern but remained below that of the uncoated sample (***Figure 45***), meaning less B was released or produced relative to the uncoated sample. While the water-extractable B of the coated sample remained similar to the uncoated one, the eluate concentration dropped to 19,591µg/L, 51,526µg/L, and 65,115µg/L at pH 10, 7, and 4, respectively, corresponding to a 1.4-1.7-fold decrease in leaching. These observations suggest that SuMo can inhibit the high leaching potential of labile element such as B in fly ash.

Similar to B, various alkali/alkaline earth metals, metalloids, and transition metals exhibited a cationic leaching pattern, wherein the leachate concentration decreased monotonically as pH increased. Among these elements, Ca was notably abundant in the uncoated Micron^3, accounting for 7.08% of total chemicals, and played a significant role in influencing leachate geochemical properties. At the natural pH (11.8), the leachate concentration of Ca was 175,048µg/L, constituting 0.2% of the total Ca. However, as the pH decreased to 10, 7, and 4, the leachate concentration of Ca increased to 945,640µg/L, 2,553,339µg/L, and 4,863,844µg/L, respectively. This inverse correlation between leachate pH and Ca concentration can be attributed to the atomic feature of Ca and geochemical changes in the sample. As an alkaline earth metal with two electrons in its outer shell, Ca was easily ionized, particularly at low pH when the redox potential increased

(***Figure 44B***). Additionally, under neutral or alkaline conditions, Ca, along with other major elements of fly ash, formed mineral precipitates, including carbonates (calcite/aragonite with Ca and dolomite/magnesite with Mg) and sulfate (anhydrite with SO_4^{2-}) ***(Garavaglia and Caramuscio, 1994; Van der Sloot et al., 1996; Fruchter et al., 1990; Mudd et al., 2004; Tian et al., 2018)***.

These undissolved minerals could immobilize various fly ash-associated elements like Cu and Zn via co-precipitation and adsorption ***(Jiao et al., 2016),*** leading to an overall reduction in mobilized elements and a decreased electrical conductivity (EC) in the eluate. When the mineral precipitates dissolved at low pH, the leachate concentration increased, resulting in the overall negative relationship between eluate pH and eluate concentration. In this study, such pH-dependent cationic leaching behavior applied to all studied alkali/alkaline earth metals (Li, Be, Mg, Ca, Sr, Ba), selected transition metals (Mn, Co, Ni, Zn, Cd), and two metalloids (B and Si), consistent with other studies ***(Lee et al. 2022; Guimaraes et al., 2016; Kim et al., 2003; Moreno et al., 2005; Ward et al., 2003; Kukier et al., 2003; Zhang et al., 2016; Zhao et al., 2020)***. Although all exhibited cationic leaching behavior, little leaching occurred at pH 8.5-12 for Co, Ni, Cd, Li, Be, Mn, and Mg due to their strong associations with alkaline minerals ***(Neupane et al., 2013),*** whereas abundant leaching occurred for major elements such as Ca, Si, and B under the same conditions. These trace elements (Co, Ni, Cd, Mn, Li, Be, and Mg) thus may not have adverse impacts on groundwater unless exposed to acidic conditions. Some studies also observed Mg and Mn as highly mobilized elements in fly ash leaching tests ***(Neupane et al., 2013),*** likely due to high variability in fly ash fractions to which elements were associated. The persistent increase in Ca, Si, and B concentration with increasing acidity in leachate indicates continuous dissolution of carbonate, sulfate, and aluminosilicate glass phase in fly ash ***(Neupane et al., 2013; Wang et al., 2004; Cetin and Aydilek, 2013)***. Along with the increased dissolution of these metal-bearing mineral phases and increased competition between H^+ and metal cations for adsorption sites, decreased sorption or association of dissolved Cd, Mg, Co, Sr, and other trace elements by the fly ash matrix occurred at lower pH levels of 1.5-6 ***(Wang et al., 2007; Izquierdo and Querol, 2012; Langmuir, 1997)***.

Similar to the uncoated sample, the LSP of Ca as a function of pH also exhibited a cationic pattern, and notably, it was lower than that of the uncoated fly ash (***Figure 45***), signifying less Ca^{2+} released or produced relative to the uncoated sample. Notably, the eluate concentration of Ca

for the coated sample at natural pH (9.1) was 575,951µg/L, 2 times higher than that of the uncoated control (175,048µg/L) at natural pH (11.8). This difference was likely a result of facilitated carbonate dissolution driven by geochemical conditions created by the polysulfide polymer layers. The observed lower natural pH for the coated fly ash leachate relative to the uncoated control indicated a larger quantity of H^+ at equilibrium, making the reaction of limestone/lime and water (**equations 1&2**) energetically favorable for producing Ca^{2+}.

$$Ca^{2+} + HCO_3 \leftrightarrow CaCO_3 \downarrow + H^+ \qquad \textbf{(2)}$$

Crucially, our results indicate that when acid was introduced to the uncoated fly ash sample, resulting in a final eluate pH of 9.1 (equivalent to a similar quantity of H^+ when SuMo fly ash leachate was at natural pH), the Ca concentration increased to 1,105,570µg/L, representing a 1.9-fold increase compared to the SuMo sample (***Figure 45***). Based on **reactions 1&2**, with the same amount of H^+ and OH^-, the observed increased Ca concentration for uncoated control can be attributed to more available CaO and $CaCO_3$, likely due to the absence of hydrophobic polysulfide coating. This pattern of reduced leaching at the same pH condition for the SuMo sample was also observed for alkali/alkaline earth metals, transient metals, and metalloids that followed the cationic leaching pattern, as shown in ***Figure 45***. With coating, the eluate concentration of these elements decreased by up to 88-fold, with a particularly large reduction of more than 5-fold occurring for Zn, Ni, Mg, Si, Cd, and Co under acid-neutral conditions. The reduced leaching potential by SuMo was not as significant for Co, Ni, and Mn at pH 4 as it was at neutral pH, possibly due to their strong association with the ferric fraction of fly ash, which is less stable under low pH conditions ***(Kukier et al., 2003)***.

Cr, Mo, and As all exhibited an oxyanionic leaching pattern for the uncoated control sample, with increased leaching under alkaline conditions. Taking Cr as an example, the eluate concentration for Cr of the uncoated control sample at natural pH (11.8) was 1,151µg/L. As pH dropped, Cr concentration in leachate remained within 880-1,560µg/L until pH reached 6. The Cr in leachate decreased to 680µg/L and 485µg/L at pH 6 and 4, respectively. Similar to our observations, ***Dubikova et al. (2006)*** reported a pH-dependent leaching pattern of Cr, reaching a low eluate concentration at near-neutral pH and a leachability plateau from pH 8 to 12. The high leachability of Cr at alkaline conditions was believed to be due to the dominance of mobile oxyanionic species, such as CrO_4^{2-} ***(Zhao et al., 2020; Shoji et al., 2002)***. As a carcinogenic substance, the leachate concentration of Cr from Micron[3] was constantly beyond the drinking

water MCL level (of 100µg/L). The increasing concentration of oxyanions at low pH was due to increased protonation of oxyanionic species that resulted in low affinity for the surface ***(Dijkstra et al., 2006)*** and facilitated dissolution of fly ash aluminosilicate particles that incorporated Cr ***(Neupane et al., 2013)***. Mo and As from the uncoated fly ash both exhibited a similar oxyanionic leaching pattern, with Mo in leachate decreasing from 1,028 to 26µg/L as pH decreased from 11.8 to 4, and As decreasing from 529 to 25µg/L as pH decreased to 6.

For the SuMo Micron^3, the LSP (liquid-to-solid partitioning) of Cr as a function of pH was completely below that for the uncoated Micron^3, indicating a decreased leaching of Cr from fly ash due to polysulfide polymer coating. When the coated fly ash leachate condition was alkaline, including the eluate own pH (9.1), the Cr in eluate was within 102-255µg/L, 3.7-12.3 time lower than those of uncoated Micron^3 eluate at the same conditions. As the eluate pH decreased to 6, Cr in coated Micron^3 eluate gradually decreased to 11µg/L and conversely increased to 178µg/L when pH further decreased to 3. Cr in SuMo Micron^3 overall exhibited an amphoteric leaching behavior, with the least leaching occurring at neutral conditions (pH 6). Such amphoteric LSP trend was observed frequently in previous studies ***(Zhao et al. 2020)***. Also, results indicate the coating effectively decreased the Cr leaching, with the highest reduction by 55-60-fold at eluate pH conditions of 6-7. At this neutral condition, coating effectively decreased the eluate concentration of Cr from being above the drinking MCL level (100µg/L) to below. The decreased leaching of Cr suggests the effectiveness of polysulfide polymer coating in reducing the available Cr for leaching, whereas the different Cr leaching behaviors of coated and uncoated Micron^3 suggest a different set of Cr species, or different precipitates that can affect Cr mobility was present owning to the presence of coating material. ***Zhao et. al (2020)*** made a similar observation, in which the majority of elements were found to have similar pH dependent LSP trends among the different ash samples, but Cr tended to have different LSP behavior due to different valence states in fly ash.

Nonetheless, distinct leaching behaviors between coated and uncoated Micron^3 were not observed for Mo and As. The similarities in leaching behavior between the coated and uncoated samples are likely due to shared controlling mechanisms, such as solubility and sorption, and common factors like leachate pH and redox potential (***Komonweeraket et al., 2015***). Mo is known to concentrate on the fly ash surface ***(Querol et al., 1995)***, with a large percentage (>51%) of Mo in Micron^3 observed to be water-extractable (***Figure 45***), and high leachability of Mo was noted across different fly ash samples and studies ***(Neupane et al., 2013)***. The significant reduction in

Mo solubility from pH 6 to 4 was likely caused by increased sorption of ferric oxyhydroxides (pH 3 to 4) and aluminum oxyhydroxides (pH 4 to 5) ***(Jones et al., 1995)***. For the oxyanionic contaminant As, previous studies employing geochemical modeling analysis have shown that the sorption-controlled leaching mechanism was mainly responsible for its leaching pattern ***(Zhang et al., 2016)***. Under alkaline conditions when the surface of fly ash was negatively charged, the sorption of oxyanions such as AsO_4^{3-}, which also have a negative charge, was not preferred, leading to high eluate concentration ***(Cornelis et al., 2008, Lee et al., 2022)***. As eluate pH increased, the adsorption of As became more significant ***(Komonweeraket et al., 2015; Zhang et al., 2016),*** resulting in a decrease in eluate concentration at neutral and low pH by more than two orders of magnitude. In this study, the eluate concentration of As was below the detection limit of 20 µg/L as long as the eluate pH was below 6. Importantly, both Mo and As showed a reduced leaching potential by 1.5-2.6-fold at neutral-alkaline conditions for SuMo Micron^3 relative to the uncoated ones (***Figure 45***).

In contrast to the previously discussed elements, despite the Micron^3 sample containing 60 mg/kg Pb (***Tables 5*** and ***6***), the leached amount across the entire tested pH range was less than 0.3%, falling below the detection limit (***Figure 46***). This aligns with previous studies indicating that Pb is highly insoluble and virtually immobile (usually less than 1%, often less than 0.1%) in both acidic and alkaline fly ash samples ***(Izquierdo and Querol, 2012)***. Pb mobilization in the leachate of coal combustion by-products was controlled by the precipitation of phosphate minerals over the pH 4-12 ***(Dubikova et al., 2006)*** and C-S-H gels formed during the hydration process of fly ash ***(Li et al., 2020)***. Abundant sulfur was detected in the leachate of the original Micron^3 (214,330-494,747 µg/L) at all pH levels, exhibiting a leaching pattern unaffected by pH and similar to previous studies ***(Kosson et al., 2009)***. Importantly, our results indicated a similar level of S was leached from the SuMo Micron^3 (***Figure 46***), suggesting limited dissolution of the polysulfide polymer coating by water.

5.2 Mercury (Hg) Volatilization Study

Leaching and volatilization experiments were carried out to evaluate the effectiveness of SuMo in reducing the diffusion and volatilization of mercury (Hg) as compared to the uncoated fly ash obtained from the sampled power plant (referred to as unclassified Class F fly ash). The leaching experiment followed the aforementioned EPA method, and Hg volatilization was evaluated at

room temperature, 73°C, 163°C, and 200°C. Changes in the total Hg content within unclassified Class F fly ash resulting from the heating treatment were employed as an indicator of Hg volatilization, addressing the challenges associated with collecting and characterizing vaporized Hg under high-temperature conditions. Leaching and volatilization experiments were carried out to evaluate the effectiveness of SuMo in reducing the diffusion and volatilization of mercury (Hg) compared to the uncoated fly ash obtained from the sampled power plant (referred to as unclassified Class F fly ash). The Hg leaching experiment followed the procedure for the previous leaching experiment, with the suspensions filtered using Supor® Membrane filters of 0.2 μm pore size. The filtrate was preserved in 5% (v/v) BrCl and stored in a 4ºC refrigerator until analysis. Hg analysis was performed using a modified EPA method 1631, involving pre-reduction with $NH_2OH{\cdot}HCl$ to eliminate excess BrCl, reduction of Hg(II) to volatile Hg(0) with $SnCl_2$, trapping, and thermo-desorption with an automated MERX purge and trap system (Brooks Rand Instruments, Seattle, WA), followed by detection on a cold-vapor atomic fluorescence spectrometer (CVAFS) ***(Zhang et al., 2021)***. The detection limit was approximately ~0.25pg/ml of Hg.

For the Hg volatilization experiment, a series of 40 mL vials were prepared, each containing 100 mg of original or SuMo fly ash samples. The experiment comprised eight duplicate groups, including four groups of original unclassified Class F fly ash samples and four groups for SuMo samples. In each group, 100 mg of fly ash samples were placed in open vials, which were then exposed to respective temperature conditions (25°C, 73°C, 163°C, and 200°C) for 30 minutes in a muffle furnace equipped with an elephant trunk ventilation system. After heating, the samples were cooled in a well-ventilated area, and septa and caps were placed on the vials to prevent any loss of fly ash or Hg. The vials were stored at room temperature for subsequent analysis. To determine the total Hg content in each sample, a digestion process was applied. The digestion process involved mixing 5mL of aqua regia (a mixture of concentrated HNO_3 and HCl in a 1:3 v/v ratio) with 100mg fly ash samples in 40mL vials. This mixture was allowed to sit for 72 hours. Subsequently, 35mL of deionized (DI) water was added, and the solid particles were removed using 0.2μm membrane filters. The Hg in the filtrate was analyzed as described above. It is worth noting that all the filters, syringes, and vials used for Hg analysis have been tested and confirmed to retain Hg at non-detectable levels.

The efficacy of SuMo in mitigating the leaching and volatilization potential of mercury (Hg) from a selected fraction (10-45 μm) of unclassified Class F fly ash was further evaluated. The total Hg content in the untreated unclassified Class F fly ash sample was 60.02±1.54μg/kg. In the absence of coating, 1-12ng/L Hg was observed in the solution (***Figure 47A***) after leaching at pH 4-11, accounting for less than 0.2% of Hg in the fly ash samples. Hg leaching was generally more pronounced under lower pH conditions than that at its own pH, with the highest leaching occurring at pH 5.6. However, with the SuMo application, the Hg concentration in the leachate ranged from 0.7-1.8ng/L, corresponding to a 1-17-fold decrease compared to the uncoated samples (***Figure 48A***). Similar to the Micron^3 sample, SuMo unclassified Class F fly ash had a lower natural eluate pH (7.6) than the uncoated one. Hg in the leachate of the coated unclassified Class F sample at natural pH was 0.7ng/L, similar to that without coating. More importantly, Hg in the leachate of the coated unclassified Class F fly ash was consistently lower than in the uncoated sample at each leaching pH condition, indicating reduced availability of Hg for leaching through coating, particularly at acidic and neutral conditions.

Fly ash utilization as fillers in plastic composites involves an injection molding process, wherein high temperatures of up to 200°C for <2 minutes can be expected. Given that Hg associated with fly ash could potentially volatilize during multiple heating conditions, the effectiveness of SuMo in mitigating Hg volatilization was further explored under various temperatures for extended time. While no Hg volatilization occurred at room temperature, approximately 19% of the Hg in unclassified Class F fly ash volatized at 73°C after 30 minutes. This percentage gradually increased to 21% at 163°C and 25% at 200°C, as depicted in ***Figure 48B***. Conversely, for SuMo unclassified Class F fly ash samples, the volatilized Hg at 73°C and 163°C were close to zero, closely matched that without any heating treatment. This suggests that Hg volatilization from fly ash under injection molding conditions can be inhibited by the polysulfide polymer coating, in contrast to untreated fly ash samples, which exhibited up to 21% Hg volatilization under the same heating conditions. However, as the heating temperature was raised to 200°C, Hg volatilization was observed with the coated sample (up to 28%), similar to the uncoated ones, suggesting the coating may degrade under higher-temperature conditions of 200°C. This aligns with previous TGA results, indicating the breakdown of coating material at 200-350°C (***Figure 16***), and highlights the correlation between effective coating and inhibited Hg volatilization under relatively low temperatures.

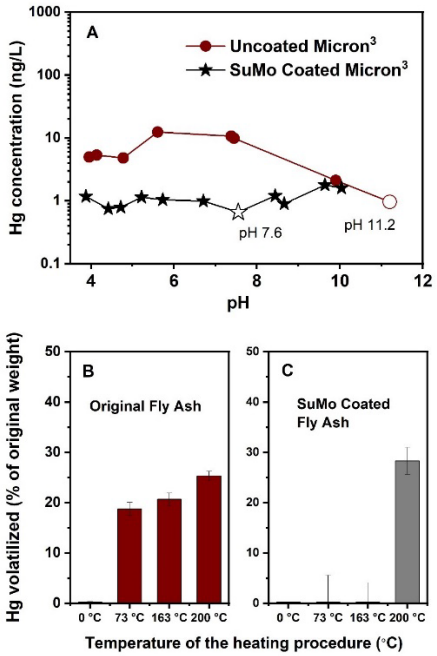

***Figure 48**. **A**) Hg leaching and **B**&**C**) Hg volatilization behavior of uncoated and SuMo-coated Boral fly ash. The eluate concentrations of uncoated and coated samples are indicated by solid red circle and black star symbols, respectively, except the data at their own pH are shown by open symbols*

5.3 Beneficial Use

An environmental characterization of SuMo fly ash was conducted using the U.S. EPA's Beneficial Uses Methodology (L/S ratio= 10, leachate collected after 24 hours). As shown in ***Table 12***, the incidence of trace elements was recorded when using SuMo fly ash as additives in elastomer, polypropylene or polyethylene, and leaching of all the COPC was below MCL.

Table 12*. A comparison of the occurrence of contaminants of interest in materials infused with the following.*

Composite type	Mercury (Hg)	Arsenic (As)	Cadmium (Cd)	Chromium (Cr)	Boron (B)	Lead (Pb)	Selenium (Se)	Reference
Maximum Contaminants Limit (Drinking Water)	**0.002 ppm**	**0.01 ppm**	**0.005 ppm**	**0.1 ppm**	**5 ppm**	**0.01 ppm**	**0.05 ppm**	
Plastic, Cermamic	-	<0.01 for both plastic and ceramic (ppm)		0.013 for ceramic, 0.007 for plastic (ppm)	-	-	<0.01 for ceramic, 0.087 for plastic (ppm)	High Strength, Encapsulated, Commercially Useful Components and Particles Made from Coal Combustion Residuals DOE Office of Fossil Energy, Award No. DE-FE0031932, X-M semiplastics
Calcium Carbonate	0.0014 (ppm)	0.0367 (ppm)	0.0005 (ppm)	0.0690 (ppm)	-	0.0005 (ppm)	-	Alicja Uliasz-Bochenczyk & Eugeniusz Mokrzycki. The potential of FBC fly ashes to reduce CO2 emission. Nature Research Scientific Reports. 2020. 10: 9469
Asphalt	0.5 (ppb)	0.6 (ppb)	-	1 (ppm)	-	-	-	S.A. Wasay (1992) Leaching behaviour of trace toxic metals from flyash, their seepage control to groundhater and utilisation of flyash, Journal of Environmental Science & Health Part A, 27:1, 25-39, DOI: 10.1080/10934529209375715
SuMo Flyash F incorporated into elastomer	<0.002 (ppm)	<0.01 (ppm)	-	<0.1 (ppm)	<1 (ppm)	<0.01 (ppm)	<0.5 (ppm)	This work
SuMo Flyash C incorporated into PP	<0.002 (ppm)	<0.001 (ppm)	<0.001 (ppm)	<0.005 (ppm)	<0.05 (ppm)	<0.001 (ppm)	<0.001 (ppm)	This work
SuMo Flyash F incorporated into PP	<0.002 (ppm)	0.001 (ppm)	<0.001 (ppm)	<0.005 (ppm)	<0.05 (ppm)	<0.001 (ppm)	<0.001 (ppm)	This work
SuMo Flyash F incorporated into PE	<0.002 (ppm)	0.007 (ppm)	<0.001 (ppm)	<0.005 (ppm)	0.09 (ppm)	<0.001 (ppm)	<0.001 (ppm)	This work
SuMo Flyash C incorporated into PE	<0.002 (ppm)	<0.001 (ppm)	<0.001 (ppm)	<0.005 (ppm)	<0.05 (ppm)	<0.001 (ppm)	<0.001 (ppm)	This work

6. PROCESS FLOW DEVELOPMENT

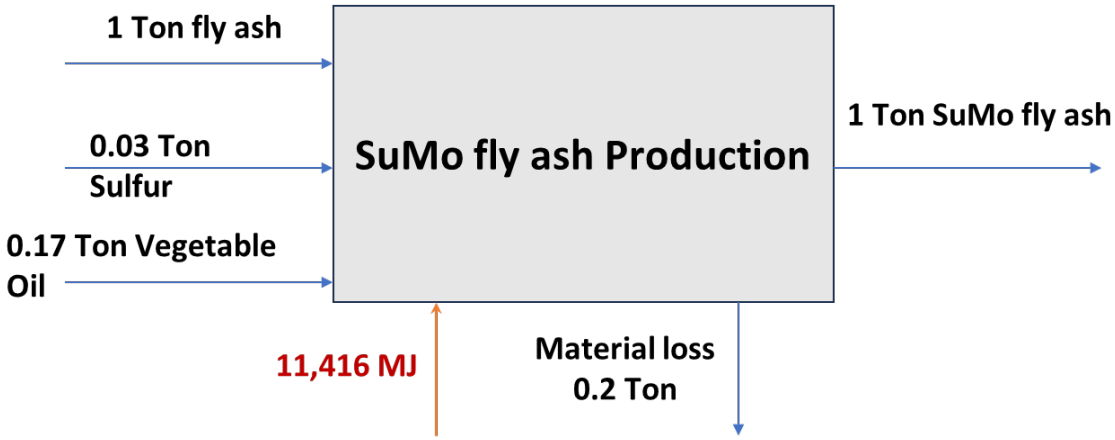

A detailed process flow sheet can be found in the Appendix A

Commercial filler price: ($CaCO_3$): 0.2 – 0.3 $/lb
Commercial filler price: (Carbon Black): 0.45 $/lb
SuMo fly ash as a filler price: 0.28 – 0.45 $/lb

Product	Carbon Footprint (kg CO_2e/ton)
$CaCO_3$	8.86
Carbon Black	1724 - 4763
SuMo Fly ash	1567

SUMMARY RESULTS

- Sulfurized Vegetable Oil-coated fly ash (SuMo fly ash) was successfully prepared with a particle size of ≤45 micron which exhibited hydrophobicity of contact angle >90º.
- The coating reduces leaching of metals (e.g., B, Cr) from fly ash when exposed to water.
- Incorporation of SuMo fly ash increases thermal stability and yield strength of plastics.
- SuMo coating helps disperse fly ash particles into the elastomer, natural rubber.
- SuMo fly ash incorporated plastic/elastomer compounds protects against leaching of toxic elements.
- SuMo fly ash price as a filler material is comparable to those for conventional filler materials.

REFERENCES

Barana, D., Orlandi, M., Salanti, A., Castellani, L., Hanel, T. and Zoia, L., 2019. Simultaneous synthesis of cellulose nanocrystals and a lignin-silica biofiller from rice husk: Application for elastomeric compounds. *Industrial Crops and Products*, 141, p.111822.

Barrera, C.S, Soboyejo, A.B.O., Cornish. K., Quantification of the contribution of filler characteristics on natural rubber reinforcement using principal component analysis. *Rubber Chemistry and Technology* 91:79-96, 2018. DOI: 10.5254/rct.82.83716

Barrera, C.S. and Cornish, K., 2016. High performance waste-derived filler/carbon black reinforced guayule natural rubber composites. *Industrial Crops and Products*, 86, pp.132-142.

Barrera, C.S., Cornish, K. Fly ash as a potential filler for the rubber industry, Chapter 25, 765-792, In: *Handbook of Fly Ash*, Kamal K. Kar (ed). Pub. Butterworth-Heinemann, an imprint of Elsevier, 2022.

Barrera, C.S., Cornish, K., Review: Characterization of agricultural and food processing residues for potential rubber filler applications. *Journal of Composites Science* 3: 102-122, 2019. doi:10.3390/jcs3040102

Chalker, J.M., Worthington, M.J., Lundquist, N.A. and Esdaile, L.J., 2019. Synthesis and applications of polymers made by inverse vulcanization. *Topics in Current Chemistry*, 377: 16

Cetin, B. and Aydilek, A.H., 2013. pH and fly ash type effect on trace metal leaching from embankment soils. *Resources, conservation and recycling*, 80, pp.107-117.

Cornelis, G., Johnson, C.A., Van Gerven, T. and Vandecasteele, C., 2008. Leaching mechanisms of oxyanionic metalloid and metal species in alkaline solid wastes: A review. *Applied Geochemistry*, 23(5), pp.955-976.

Cox, J.A., Lundquist, G.L., Przyjazny, A. and Schmulbach, C.D., 1978. Leaching of boron from coal ash. *Environmental Science & Technology*, 12(6), pp.722-723.

Das, A. and Satapathy, B.K., 2011. Structural, thermal, mechanical and dynamic mechanical properties of cenosphere filled polypropylene composites. *Materials & Design*, 32(3), pp.1477-1484.

Deepthi, M.V., Sharma, M., Sailaja, R.R.N., Anantha, P., Sampathkumaran, P. and Seetharamu, S., 2010. Mechanical and thermal characteristics of high density polyethylene–fly ash cenospheres composites. *Materials & Design*, 31(4), pp.2051-2060

Dixon, D.A., Zeroka, D.J., Wendoloski, J.J. and Wasserman, Z.R., 1985. The molecular structure of hydrogen disulfide (H2S2) and barriers to internal rotation. *The Journal of Physical Chemistry*, 89(25), pp.5334-5336.

Dubikova, M., Jankowski, J., Ward, C.R., French, D., 2006. Modelling element mobility in water-fly ash interactions. Co-operative Research Centre for Coal in Sustainable Development. Research Report.

Dijkstra, J.J., Van der Sloot, H.A. and Comans, R.N., 2006. The leaching of major and trace elements from MSWI bottom ash as a function of pH and time. *Applied Geochemistry*, 21(2), pp.335-351.

EPRI, Program on Technology Innovation: *Alternative and Innovative Technologies for Coal Combustion Product Management*. EPRI, Palo Alto, CA: 2016. 3002009569.

Fan, Y., Fowler, G.D. and Zhao, M., 2020. The past, present and future of carbon black as a rubber reinforcing filler–A review. *Journal of cleaner production*, 247, p.119115.

Fruchter, J.S., Rai, D. and Zachara, J.M., 1990. Identification of solubility-controlling solid phases in a large fly ash field lysimeter. *Environmental Science & Technology*, 24(8), pp.1173-1179.

Garavaglia, R. and Caramuscio, P., 1994. Coal fly-ash leaching behaviour and solubility controlling solids. *Studies in Environmental Science*. 60: pp. 87-102.

Ghosh, T. and Karak, N., 2018. Biobased multifunctional macroglycol containing smart thermoplastic hyperbranched polyurethane elastomer with intrinsic self-healing attribute. *ACS Sustainable Chemistry & Engineering*, 6(3), pp.4370-4381.

Guimaraes, M. and Ladwig K., 2016. Program on Technology Innovation: *Alternative and Innovative Technologies for Coal Combustion Product Management*. 3002009569.

IkhtiarBakti, A. and Gareso, P.L., 2018. Characterization of active carbon prepared from coconuts shells using FTIR, XRD and SEM techniques. *Jurnal ilmiah pendidikan fisika* Al-Biruni, 7(1), pp.33-39.

Iwashita, A., Sakaguchi, Y., Nakajima, T., Takanashi, H., Ohki, A. and Kambara, S., 2005. Leaching characteristics of boron and selenium for various coal fly ashes. *Fuel*, 84(5), pp.479-485.

Izquierdo, M. and Querol, X., 2012. Leaching behaviour of elements from coal combustion fly ash: an overview. *International Journal of Coal Geology*, 94, pp.54-66

James, W.D., Graham, C.C., Glascock, M.D. and Hanna, A.S.G., 1982. Water-leachable boron coal ashes. *Environmental Science & Technology*, 16(4), pp.195-197.

Jiao, F., Zhang, L., Dong, Z., Namioka, T., Yamada, N. and Ninomiya, Y., 2016. Study on the species of heavy metals in MSW incineration fly ash and their leaching behavior. *Fuel Processing Technology*, 152, pp.108-115.

Jones, D.R., 1995. The leaching of major and trace elements from coal ash. In *Environmental aspects of trace elements in coal*, (pp. 221-262.). Dordrecht: Springer Netherland.

Kukier, U., Ishak, C.F., Sumner, M.E. and Miller, W.P., 2003. Composition and element solubility of magnetic and non-magnetic fly ash fractions. *Environmental Pollution*, 123(2), pp.255-266.

Komonweeraket, K., Cetin, B., Benson, C.H., Aydilek, A.H. and Edil, T.B., 2015. Leaching characteristics of toxic constituents from coal fly ash mixed soils under the influence of pH. *Waste Management*, 38, pp.174-184.

Khosla, B.K., Gupta, R.K. and Abrol, I.P., 1979. Salt leaching and the effect of gypsum application in a saline-sodic soil. Agricultural Water Management, 2(3), pp.193-202.

Kim, A.G., Kazonich, G. and Dahlberg, M., 2003. Relative solubility of cations in Class F fly ash. *Environmental Science & Technology*, 37(19), pp.4507-4511.

Kutchko, B. G., & Kim, A. G. (2006). Fly ash characterization by SEM– EDS. *Fuel*, 85(17-18), 2537-2544. 2.

Komonweeraket, K., Cetin, B., Benson, C.H., Aydilek, A.H. and Edil, T.B., 2015. Leaching characteristics of toxic constituents from coal fly ash mixed soils under the influence of pH. *Waste Management*, 38, pp.174-184.

Kosson, D., Sanchez, F., Kariher, P., Turner, L.H., Delapp, R. and Seignette, P.F.A.B., 2009. *Characterization of coal combustion residues from electric utilities—leaching and*

characterization data. EPA Office of Research and Development, Ed. National Risk Management and Research Laboratory, Research Triangle Park, NC.

Langmuir, D., 1997. *Aqueous Environmental Geochemistry*. Prentice Hall: Upper Saddle River, NJ, 600.

Lee, H., Coulon, F. and Wagland, S.T., 2022. Influence of pH, depth and humic acid on metal and metalloids recovery from municipal solid waste landfills. *Science of The Total Environment*, 806, p.150332.

Li, J., Zhang, S., Wang, Q., Ni, W., Li, K., Fu, P., Hu, W. and Li, Z., 2020. Feasibility of using fly ash–slag-based binder for mine backfilling and its associated leaching risks. *Journal of Hazardous Materials*, 400, p.123191.

Maurya, A.K., Gogoi, R., Sethi, S.K. and Manik, G., 2021. A combined theoretical and experimental investigation of the valorization of mechanical and thermal properties of the fly ash-reinforced polypropylene hybrid composites. *Journal of Materials Science*, 56(30), pp.16976-16998.

Mahasti, N.N., Lin, J.Y., Huang, Y.J., Wu, J.Y., Yen, M.C., Chiu, Y.H. and Huang, Y.H., 2022. Effective boron removal from synthetic wastewater by multi-stage calcium-based chemical oxo-precipitation process. *Journal of Cleaner Production*, 380, p.134956.

Moreno, N., Querol, X., Andrés, J.M., Stanton, K., Towler, M., Nugteren, H., Janssen-Jurkovicová, M. and Jones, R., 2005. Physico-chemical characteristics of European pulverized coal combustion fly ashes. *Fuel*, 84(11), pp.1351-1363.

Mudd, G.M., Weaver, T.R. and Kodikara, J., 2004. Environmental geochemistry of leachate from leached brown coal ash. *Journal of Environmental Engineering*, 130(12), pp.1514-1526.

Nishal, V., Kumar, A., Kadyan, P.S., Singh, D., Srivastava, R., Singh, I. and Kamalasanan, M.N., 2013. Synthesis, characterization, and electroluminescent characteristics of mixed-ligand zinc (II) complexes. Journal of electronic materials, 42, pp.973-978.

Neupane, G. and Donahoe, R.J., 2013. Leachability of elements in alkaline and acidic coal fly ash samples during batch and column leaching tests. *Fuel*, 104, pp.758-770.

Querol, X., Fernández-Turiel, J. and López-Soler, A., 1995. Trace elements in coal and their behaviour during combustion in a large power station. *Fuel*, 74(3), pp.331-343.

Ren, X., Barrera, C.S., Tardiff, J.L., Gil, A. and Cornish, K., 2020. Liquid guayule natural rubber, a renewable and crosslinkable processing aid in natural and synthetic rubber compounds. Journal of Cleaner Production, 276, p.122933.

Ren, X., Cornish, K., Eggshell improves dynamic properties of durable guayule rubber composites co-reinforced with silanized silica. *Industrial Crops and Products* 138: 111440, 2019 https://doi.org/10.1016/j.indcrop.2019.06.003

Ren, X. and Sancaktar, E., 2019. Use of fly ash as eco-friendly filler in synthetic rubber for tire applications. *Journal of cleaner production*, 206, pp.374-382.

Roy, W.R. and Berger, P.M., 2011. Geochemical controls of coal fly ash leachate pH. *Coal Combustion and Gasification Products*, 3(4), pp.63-66.

Salaeh, S. and Nakason, C., 2012. Influence of modified natural rubber and structure of carbon black on properties of natural rubber compounds. *Polymer composites*, 33(4), pp.489-500.

Satapathy, S. and Kothapalli, R.V., 2018. Mechanical, dynamic mechanical and thermal properties of banana fiber/recycled high density polyethylene biocomposites filled with flyash cenospheres. *Journal of Polymers and the Environment,* 26, pp.200-213.

Sear, L.K., Weatherley, A.J. and Dawson, A., 2003, October. *The environmental impacts of using fly ash–The UK producers' perspective*. In Proceedings of International Ash Utilisation Symposium, Lexington, Kentucky.

Sengupta, S., Ray, D. and Mukhopadhyay, A., 2013. Sustainable materials: value-added composites from recycled polypropylene and fly ash using a green coupling agent. *ACS Sustainable Chemistry & Engineering*, 1(6), pp.574-584.

Sombatsompop, N., Thongsang, S., Markpin, T. and Wimolmala, E., 2004. Fly ash particles and precipitated silica as fillers in rubbers. I. Untreated fillers in natural rubber and styrene–butadiene rubber compounds. *Journal of Applied Polymer Science*, 93(5), pp.2119-2130.

Shoji, T., Huggins, F.E., Huffman, G.P., Linak, W.P. and Miller, C.A., 2002. XAFS spectroscopy analysis of selected elements in fine particulate matter derived from coal combustion. *Energy & Fuels*, 16(2), pp.325-329.

Thongsang, S. and Sombatsompop, N., 2006. Effect of NaOH and Si69 treatments on the properties of fly ash/natural rubber composites. Polymer composites, 27(1), pp.30-40.

Tian, Q., Guo, B., Nakama, S. and Sasaki, K., 2018. Distributions and leaching behaviors of toxic elements in fly ash. *Acs Omega*, 3(10), pp.13055-13064.

Van der Sloot, H.A., Comans, R.N.J. and Hjelmar, O., 1996. Similarities in the leaching behaviour of trace contaminants from waste, stabilized waste, construction materials and soils. *Science of the Total Environment*, 178(1-3), pp.111-126.

Ward, C.R., French, D.H. and Jankowski, J., 2003. *Comparative evaluation of leachability test methods and element mobility for selected Australian fly ash samples*. Pittsburgh, Pa., Pittsburgh Coal Conference.

Wang, J., Teng, X., Wang, H. and Ban, H., 2004. Characterizing the metal adsorption capability of a Class F coal fly ash. *Environmental Science & Technology*, 38(24), pp.6710-6715.

Wang, T., Wang, J., Burken, J.G., Ban, H. and Ladwig, K., 2007. The leaching characteristics of selenium from coal fly ashes. *Journal of Environmental Quality*, 36(6), pp.1784-1792.

Worthington, M.J., Kucera, R.L., Albuquerque, I.S., Gibson, C.T., Sibley, A., Slattery, A.D., Campbell, J.A., Alboaiji, S.F., Muller, K.A., Young, J. and Adamson, N., 2017. Laying waste to mercury: inexpensive sorbents made from sulfur and recycled cooking oils. *Chemistry–A European Journal*, 23(64), pp.16219-16230.

Yüksel, S., & Yürüm, Y. (2009). Removal of boron from aqueous solutions by adsorption using fly ash, zeolite, and demineralized lignite. *Separation Science and Technology*, 45(1), 105-115.

Zhang, Y., Cetin, B., Likos, W.J. and Edil, T.B., 2016. Impacts of pH on leaching potential of elements from MSW incineration fly ash. *Fuel*, 184, pp.815-825.

Zhang, L., Liang, X., Wang, Q., Zhang, Y., Yin, X., Lu, X., Pierce, E.M. and Gu, B., 2021. Isotope exchange between mercuric [Hg (II)] chloride and Hg (II) bound to minerals and thiolate ligands: Implications for enriched isotope tracer studies. *Geochimica et Cosmochimica Acta*, 292, pp.468-481.

Zhao, L., Dai, S., Finkelman, R.B., French, D., Graham, I.T., Yang, Y., Li, J. and Yang, P., 2020. Leaching behavior of trace elements from fly ashes of five Chinese coal power plants. *International Journal of Coal Geology*, 219, p.103381

Zhu, Z., Wang, X., Dai, S., Huang, B., & He, Q. (2013). Fractional characteristics of coal fly ash for beneficial use. *Journal of materials in civil engineering*, 25(1), 63-69

APPENDIX A: Details of sub-task 5.3

Details of sub-task 5.3

Assumptions
Pre-washed water will be neutralized with flyash's leachate
Cost is about 0.16$/lb for a 2 minute thinky mixer, and about 0.25$/lb for 4 minutes thinky mixer
Toluene cost is negligible because it can be evaporated and recaptured
Used cooking oil price 825$/tonne

Pricing of Chemicals	
Soda Ash Price	0 $/kg
Elemental S	0.15 $/kg
Price VO* (lb):	0.30 $/lb
Price VO (g):	0.0001 $/g
KOH	2.32 $/kg
NaOH	0.56 $/kg
Acetic acid	0.81 $/kg
Water	0.8 $/kg
Waste Water treatment	0.1 $/kg
HCl	0.15 $/kg
Waste Cooking Oil	0.2 $/lb
Canola Oil	0.47 $/lb
Corn Oil	0.62 $/lb
Soybean Oil	0.44 $/lb
*waste cooking oil price	

Cp (Specific heat)	
Flyash	0.72 J/g/.K
Vegetable oil	0.167 J/g/.K
Elemental S	0.71 J/g/.K
SuMo Flyash	0.66 J/g/.K

Q (J) =	m*Cp*(T-Troom)
SVO (Specific Heat)	0.2376 J/g.K
SuMo Flyash (Specific Heat)	0.6573 J/g.K

Energy Conversion	
1 kJ =	2.78E-04 kWh
Electricity Market Price	0.103 $/kWh

Fly ash pre-washing step:

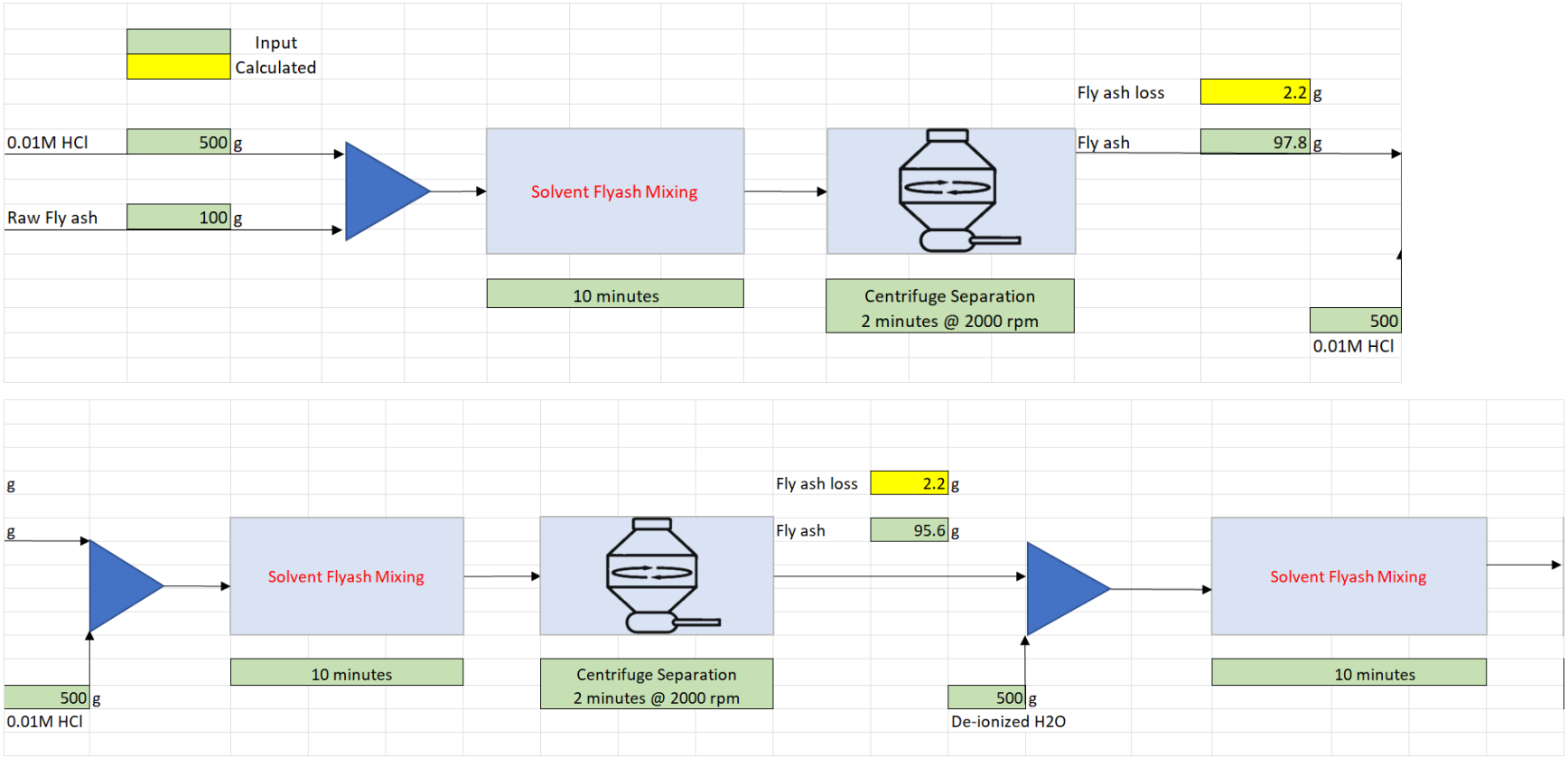

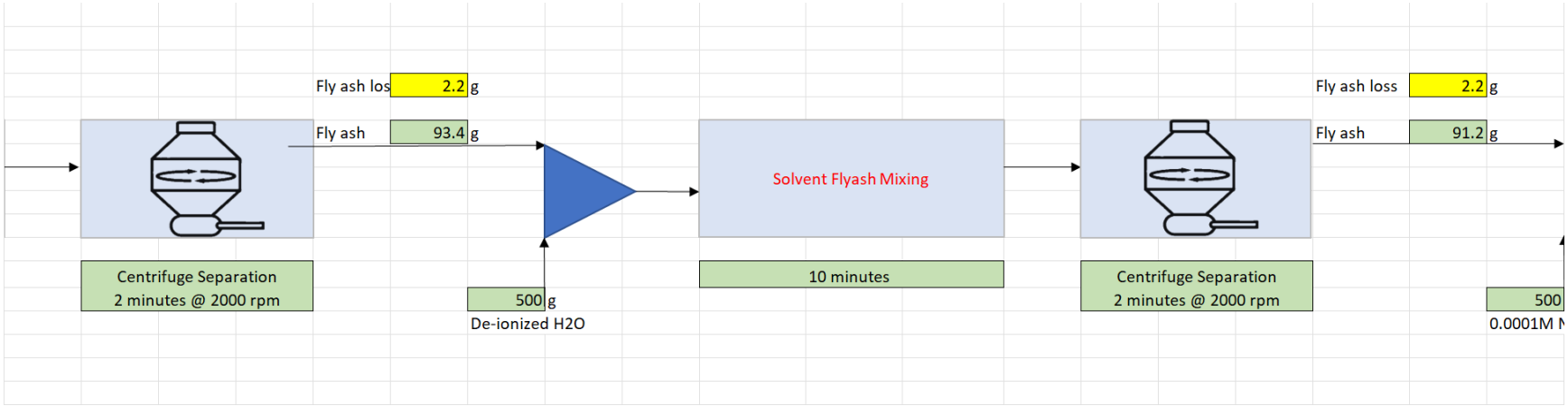
Fly ash los
2.2 g
Fly ash
93.4 g
Centrifuge Separation
2 minutes @ 2000 rpm
500 g
De-ionized H2O
Solvent Flyash Mixing
10 minutes
Fly ash loss
2.2 g
Fly ash
91.2 g
Centrifuge Separation
2 minutes @ 2000 rpm
500
0.0001M N

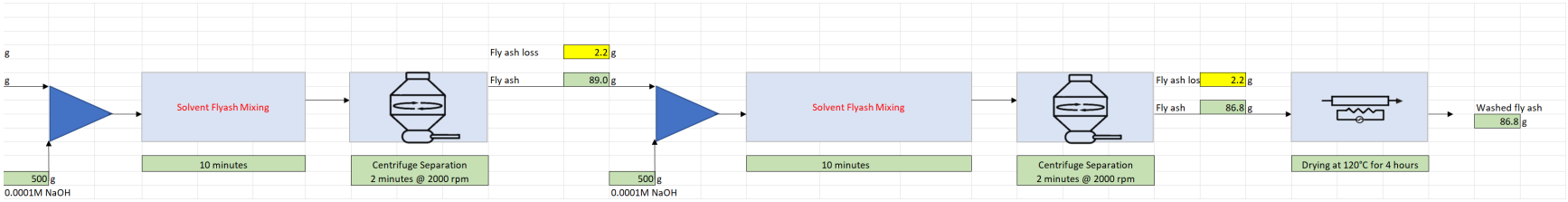
g
g
500 g
0.0001M NaOH
Solvent Flyash Mixing
10 minutes
Centrifuge Separation
2 minutes @ 2000 rpm
Fly ash loss
2.2 g
Fly ash
89.0 g
500 g
0.0001M NaOH
Solvent Flyash Mixing
10 minutes
Centrifuge Separation
2 minutes @ 2000 rpm
Fly ash los
2.2 g
Fly ash
86.8 g
Drying at 120°C for 4 hours
Washed fly ash
86.8 g

Synthesis of SuMo fly ash

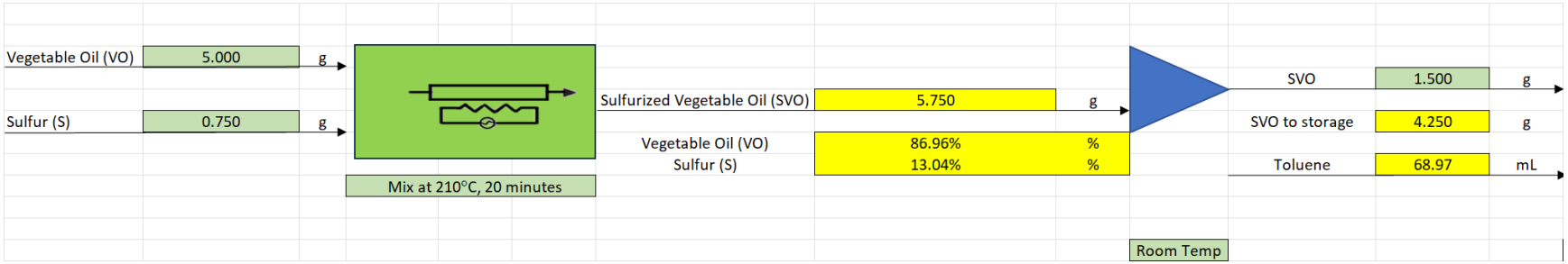

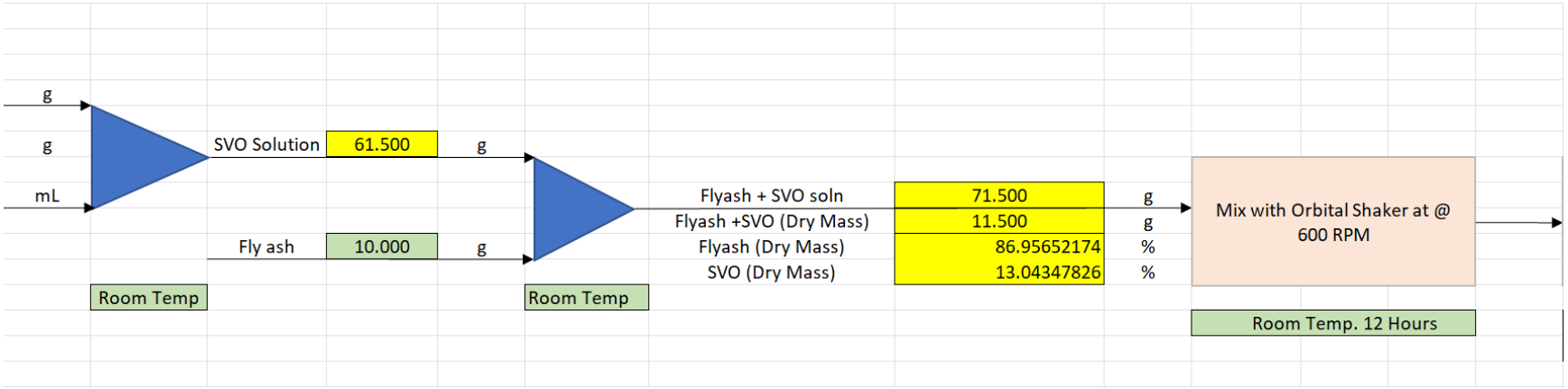

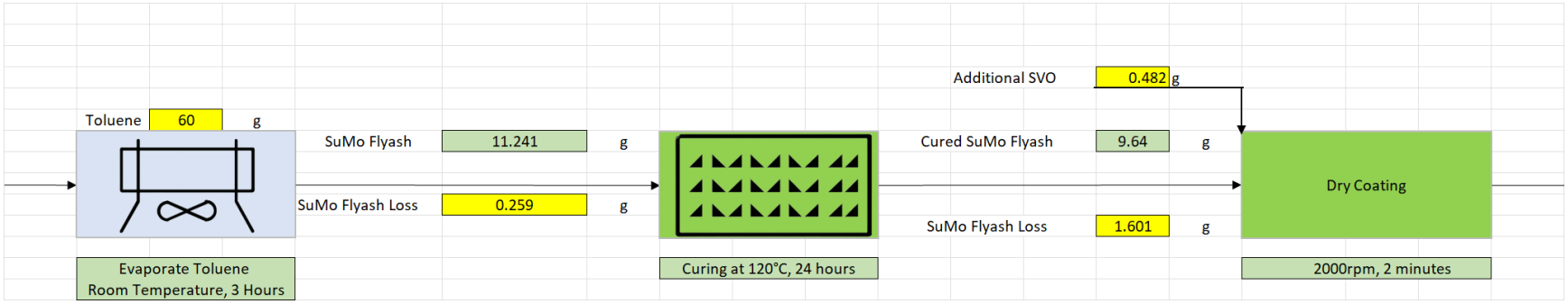
Toluene
60
g
SuMo Flyash
11.241
g
SuMo Flyash Loss
0.259
g
Additional SVO
0.482
g
Cured SuMo Flyash
9.64
g
SuMo Flyash Loss
1.601
g
Dry Coating
Evaporate Toluene
Room Temperature, 3 Hours
Curing at 120°C, 24 hours
2000rpm, 2 minutes

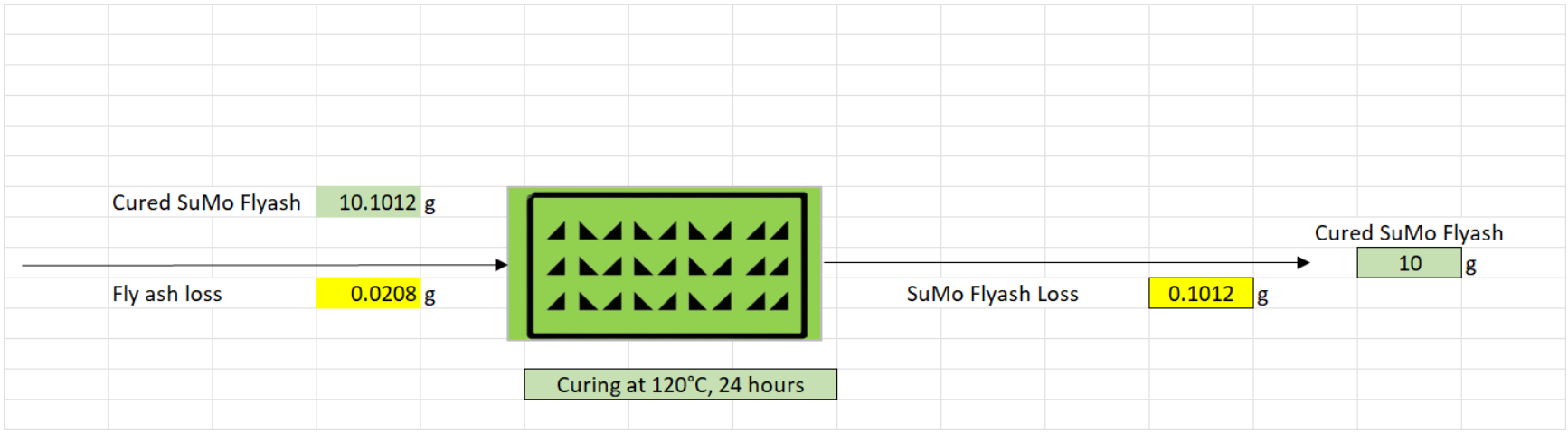
Cured SuMo Flyash
10.1012
g
Fly ash loss
0.0208
g
SuMo Flyash Loss
0.1012
g
Cured SuMo Flyash
10
g
Curing at 120°C, 24 hours

Overall Heat and Material Balance and Costing

Overview
*Cycle = Sum of all acid, water, and base washes per batch
*Wash = A singular wash of fly ash, regardless of type

Prewash Materials	*Starting amount*	*Unit*	*Market Price*	*Unit*	*Cost*
Fly Ash:	0.100	kg	0.093	$/kg	0.0093
HCl	3.65E-04	kg	0.15	$/kg	5.47E-05
H2O	3.000	kg	0.000375	$/kg	0.001125
NaOH	4.00E-06	kg	0.56	$/kg	2.240E-06
Assumed fly ash lost per cycle	13.22	%	-	-	-
			Total:	0.0105	$

Fly Ash Coating (SVO Used)	*Starting amount*	*Unit*	*Market Price*	*Unit*	*Cost*
Washed Flyash	0.01	kg	0.120787353	$/kg	1.208E-03
SVO Used (Wet coating ratio)	0.0015	kg	0.737	$/kg	1.106E-03
Assumed FA lost per wet coat	16.17	%	-	-	-
SVO Used (Dry coating ratio)	0.00048	kg	0.737	$/kg	3.554E-04
Assumed FA lost per dry coat/cure	1.205	%	-	-	-
			Total:	0.002669	$

*Note: This SVO is for total amount made, some of which is used, some of which is put into storage

SVO Sythesis					
	Starting amount	*Unit*	*Market Price*	*Unit*	*Cost*
Vegetable Oil	0.005	kg	0.825	$/kg	0.004125
Sulfur (elemental)	0.00075	kg	0.15	$/kg	1.13E-04
Energy	1.700E-05	kWh	0.103	$/kWh	1.751E-06
			Total:	0.004239	$

Energy Cost					
	Energy Required per 10g Cured SuMo FA	*Unit*	*Market Price*	*Unit*	*Cost*
Wet Coat Curing	4.94E-03	kWh	0.103	$/kWh	5.09E-04
Dry Coat Curing	4.44E-03	kWh	0.103	$/kWh	4.57E-04
Thinky Mixer	2.00E-02	kWh	0.103	$/kWh	2.06E-03
Orbital Mixer	5.62E-03	kWh	0.103	$/kWh	5.79E-04
			Total:	0.003605	$

Industry Standards		
Price Oil Used	0.375	$/lb
Wattage of Orbital Shaker used	75	W
**Edit these values to get different cost predictions*		

Prewash Costs		
Amount of flyash washed	0.08678	kg
Price to wash flyash	0.120787	$/kg
Minimum Cost (Waste Oil, 75W shakerpower)	0.285181	$/lb
Maximum Cost (Fresh Oil, 75W shaker power)	0.454937	$/lb

Total Costs		
Total production cost	0.006274	$
Amount of flyash produced	0.0100	kg
Unit cost per kg of SuMo FA	0.6274	$/kg
Unit cost per lb of SuMo FA	0.285181	$/lb

APPENDIX B: Technology Maturation Plan

TECHNOLOGY MATURATION PLAN

for

AOI-1: Surface Modified Fly Ash for Value Added Products (SuMo Fly Ash)

Grant Period: September 1, 2021 to January 31, 2024

DOE Award Number: DE-FE0002309

SUBMITTED BY

University of Illinois at Urbana-Champaign
Prairie Research Institute - Illinois Sustainable Technology Center
1 Hazelwood Drive
Champaign, IL 61820-7465

Principal Investigator
Chinmoy Baroi, PhD

Phone: 217-244-1709
Fax: 217-333-8944
Email: cbaroi@illinois.edu

SUBMITTED TO

U.S. Department of Energy
National Energy Technology Laboratory
Office of Fossil Energy

A. TECHNOLOGY READINESS LEVEL

TRL of the Technology at the beginning and end of the project

The project technology at the beginning of the project was at TRL-2. The scientific principles behind the technology are well known and shown to be applicable to the process under consideration. Results of the project work performed by us and presented in the Project final report have been promising and determined to be a plausible approach.

In the project we addressed the following questions:

(a) What is the minimum quantity of VO/FA and sulfur needed to minimize leaching of constituents of potential concern (COPCs) below EPA threshold levels?

(b) How do the properties of SuMo fly ash differ from untreated unmodified fly ash?

(c) What are the chemical interactions between the modified fly ash and different polymeric matrices (thermoplastics, elastomers, and thermosets)

(d) What is the effect of modified fly ash size and size range on polymer composite performance? Does modification allow a greater particle size range to be used than possible with unmodified fly ash?

(e) What coating techniques are most cost-effective for scale-up?

The project technology is now at TRL-4, with the answers to all the above questions, which are included in the final report.

Target Commercial Application

SuMo fly ash developed and matured in this project, addresses the need to increase the beneficial utilization of coal combustion residuals (CCR), thereby minimizing the volume of CCR landfills while protecting the environment and the health and safety of the public. More specifically, this project will innovate, develop, and subsequently deploy next-generation fly ash

beneficiation materials with improved cost and performance by creating hydrophobic fly ash with minimum leaching potential and validation as high-value fillers in polymeric products. By creating a high-value product, SuMo fly ash overcame some of the inherent barriers to fly ash utilization, such as regional and seasonal imbalances in supply and demand, and transportation and beneficiation costs. SuMo fly ash offers the following benefits over conventional fly ash: (a) reduced leaching potential (b) higher value, so increased revenue from its sale (c) savings and better performance as fillers in polymers with improved strength, durability, and workability, (d) satisfying criteria laid out in the EPA beneficial use rule, (d) no additional environmental impacts due to incorporation of SuMo fly ash.

The SuMo fly ash incorporated plastics and elastomers also showed better structural properties as compared to those for the regular commercial fillers (e.g., $CaCO_3$ for plastics and Carbon Black for elastomers).

In the U.S. in 2022, 28.2 million tons (Mt) of fly ash were produced. 16.8 Mt of fly ash were utilized (no plastic/elastomer filler application). At the same year, in North America, 3.92 Mt calcium carbonate ($CaCO_3$) were produced. At that same year, in the U.S., 1.6 Mt Carbon Black reinforcing fillers were produced (globally 14.5 Mt, at a value of $16.5B). Most of the Calcium Carbonate filler market and part of the Carbon Black filler market can be replaced by SuMo fly ash fillers. Based on the project results, fly ash utilization can be increased from ~60% to 75%.

B. POST-PROJECT PLANS

The process flow sheet and heat and material balance developed under sub-task 5.3 will serve as the basis for further process optimization to refine the process further (upon availability of future funding). Based on this, an integrated set-up for SuMo fly ash preparation will be designed and built to reach TRL-5 (upon availability of new funding).